



BRÖSTCANCER
FÖRBUNDET

Forskningsrapport



Huvudsökande:

Balazs Acs

MD, PhD

Karolinska Institutet och Karolinska Universitetssjukhuset, Stockholm

Frågeställning:

Kan vi förbättra rutinmässig klinisk patologi i bröstcancerdiagnostik?

Tre frågor till Balazs:

Hur kan resultatet av er forskning hjälpa patienterna, rent konkret?

Histopatologisk bedömning av tumörer ger information som är avgörande för kliniskt beslutsfattande. Dagens cancerdiagnostik utförs manuellt av patologer med hjälp av ett mikroskop eller digitaliserade bilder. I analysen ingår noggrann morfologisk bedömning av tumörtyp, grad och biomarkörer. Men mänskliga bedömningar är kopplade till hög grad av osäkerhet och variation, vilket ibland ger opålitlig information som leder till suboptimala behandlingsbeslut. Dagens oprecisa cancerdiagnostik leder till under- och överbehandling som påverkar patientens resultat och skapar en ohållbar kostnad för samhället.

Vi utvecklade datorbaserade modeller med hjälp av artificiell intelligens (AI, maskininläring) för bedömning av histopatologibilder, som syftar till att förbättra rutinmässig klinisk patologi. Fokus låg på bedömning av mest problematiska biomarkörer (t. ex: Ki67, sTILs) med syfte att fungera som beslutsstöd till patologen. Vi har skapat en artificiell intelligens baserad algoritm för bedömning av sTILs i bröstcancer. Denna algoritm användes för att mäta sTILs i den randomiserade fas II-studien Scandinavian Breast Group 2004-1.

Dessutom har vi också utvecklat ett AI-verktyg för den internationella arbetsgruppen för Ki67 i bröstcancer för att bedöma typen av biopsi och dess effekt på Ki67-reproducerbarheten.

Hur viktigt har stödet från Bröstcancerförbundet varit för er forskning?

Stödet var avgörande för mig och mina kollegor. Utan Bröstcancerförbundets generösa bidrag hade vi inte kunnat starta projektet.

Vad vill du hälsa alla Bröstcancerförbundets givare?

Era bidrag gör skillnad! Jag vill hälsa att alla bidrag möjliggör att utveckla den kliniska bröstcancerforskningen i Sverige. Genom att skänka pengar till Bröstcancerförbundet bidrar man till att vi ska kunna erbjuda ännu bättre diagnostik och behandling för våra patienter.

På efterföljande sidor finns Balazs publikationer för dig som vill läsa mer.

ARTICLE OPEN



Systematically higher Ki67 scores on core biopsy samples compared to corresponding resection specimen in breast cancer: a multi-operator and multi-institutional study

Balazs Acs ^{1,2,3}✉, Samuel C. Y. Leung⁴, Kelley M. Kidwell⁵, Indu Arun⁶, Renaldas Augulis ⁷, Sunil S. Badve ⁸, Yalai Bai¹, Anita L. Bane⁹, John M. S. Bartlett^{10,11}, Jane Bayani¹⁰, Gilbert Bigras¹², Annika Blank^{13,14}, Henk Buikema¹⁵, Martin C. Chang¹⁶, Robin L. Dietz ¹⁷, Andrew Dodson¹⁸, Susan Fineberg¹⁹, Cornelia M. Focke²⁰, Dongxia Gao⁴, Allen M. Gown ²¹, Carolina Gutierrez ²², Johan Hartman ^{2,3}, Zuzana Kos²³, Anne-Vibeke Lænkholm²⁴, Arvydas Laurinavicius ⁷, Richard M. Levenson ²⁵, Rustin Mahboubi-Ardakani²⁵, Mauro G. Mastropasqua ²⁶, Sharon Nofech-Mozes²⁷, C. Kent Osborne²², Frédérique M. Penault-Llorca^{28,29}, Tammy Piper¹¹, Mary Anne Quintayo¹⁰, Tilman T. Rau^{13,30}, Stefan Reinhard ¹³, Stephanie Robertson ^{2,3}, Roberto Salgado ^{31,32}, Tomoharu Sugie³³, Bert van der Vegt ¹⁵, Giuseppe Viale^{26,34}, Lila A. Zabaglo³⁵, Daniel F. Hayes ³⁶, Mitch Dowsett ³⁵, Torsten O. Nielsen ⁴, David L. Rimm ¹✉ and on behalf of the International Ki67 in Breast Cancer Working Group of the Breast International Group and North American Breast Cancer Group (BIG-NABCG)*

© The Author(s) 2022

Ki67 has potential clinical importance in breast cancer but has yet to see broad acceptance due to inter-laboratory variability. Here we tested an open source and calibrated automated digital image analysis (DIA) platform to: (i) investigate the comparability of Ki67 measurement across corresponding core biopsy and resection specimen cases, and (ii) assess section to section differences in Ki67 scoring. Two sets of 60 previously stained slides containing 30 core-cut biopsy and 30 corresponding resection specimens from 30 estrogen receptor-positive breast cancer patients were sent to 17 participating labs for automated assessment of average Ki67 expression. The blocks were centrally cut and immunohistochemically (IHC) stained for Ki67 (MIB-1 antibody). The QuPath platform was used to evaluate tumoral Ki67 expression. Calibration of the DIA method was performed as in published studies. A guideline for building an automated Ki67 scoring algorithm was sent to participating labs. Very high correlation and no systematic error ($p = 0.08$) was found between consecutive Ki67 IHC sections. Ki67 scores were higher for core biopsy slides compared to paired whole sections from resections ($p \leq 0.001$; median difference: 5.31%). The systematic discrepancy between core biopsy and corresponding whole sections was likely due to pre-analytical factors (tissue handling, fixation). Therefore, Ki67 IHC should be tested on core biopsy samples to best reflect the biological status of the tumor.

Modern Pathology (2022) 35:1362–1369; <https://doi.org/10.1038/s41379-022-01104-9>

¹Department of Pathology, Yale University School of Medicine, New Haven, CT, USA. ²Department of Oncology and Pathology, Karolinska Institutet, Stockholm, Sweden. ³Department of Clinical Pathology and Cancer Diagnostics, Karolinska University Hospital, Stockholm, Sweden. ⁴University of British Columbia, Vancouver, BC, Canada. ⁵Department of Biostatistics, School of Public Health, University of Michigan, Ann Arbor, MI, USA. ⁶Tata Medical Center, Kolkata, West Bengal, India. ⁷Vilnius University Faculty of Medicine and National Center of Pathology, Vilnius University Hospital Santaros Clinics, Vilnius, Lithuania. ⁸Department of Pathology and Laboratory Medicine, Emory University School of Medicine, Atlanta, GA, USA. ⁹Juravinski Hospital and Cancer Centre, McMaster University, Hamilton, ON, Canada. ¹⁰Ontario Institute for Cancer Research, Toronto, ON, Canada. ¹¹Edinburgh Cancer Research Centre, Western General Hospital, Edinburgh, United Kingdom. ¹²Department of Laboratory Medicine and Pathology, University of Alberta, Edmonton, AB, Canada. ¹³Institute of Pathology, University of Bern, Bern, Switzerland. ¹⁴Institute of Pathology, Triemli Hospital Zurich, Zurich, Switzerland. ¹⁵University of Groningen, University Medical Center Groningen, Groningen, The Netherlands. ¹⁶Department of Pathology & Laboratory Medicine, University of Vermont Medical Center, Burlington, VT, USA. ¹⁷Department of Pathology, Olive View-UCLA Medical Center, Los Angeles, CA, USA. ¹⁸UK NEQAS for Immunocytochemistry and In-Situ Hybridisation, London, United Kingdom. ¹⁹Montefiore Medical Center and the Albert Einstein College of Medicine, Bronx, NY, USA. ²⁰Dietrich-Bonhoeffer Medical Center, Neubrandenburg, Mecklenburg-Vorpommern, Germany. ²¹PhenoPath Laboratories, Seattle, WA, USA. ²²Lester and Sue Smith Breast Center and Dan L. Duncan Comprehensive Cancer Center, Baylor College of Medicine, Houston, TX, USA. ²³Department of Pathology and Laboratory Medicine, University of British Columbia, Vancouver, BC, Canada. ²⁴Department of Surgical Pathology, Zealand University Hospital, Roskilde, Denmark. ²⁵Department of Medical Pathology and Laboratory Medicine, University of California Davis Medical Center, Sacramento, CA, USA. ²⁶European Institute of Oncology, Milan, Italy. ²⁷University of Toronto Sunnybrook Health Sciences Centre, Toronto, ON, Canada. ²⁸Imagerie Moléculaire et Stratégies Théranostiques, UMR1240, Université Clermont Auvergne, INSERM, Clermont-Ferrand, France. ²⁹Service de Pathologie, Centre Jean PERRIN, Clermont-Ferrand, France. ³⁰Institute of Pathology, Heinrich Heine University and University Hospital of Duesseldorf, Duesseldorf, Germany. ³¹Department of Pathology, GZA-ZNA, Antwerp, Belgium. ³²Peter MacCallum Cancer Centre, University of Melbourne, Melbourne, VIC, Australia. ³³Kansai Medical University, Hirakata, Osaka, Japan. ³⁴European Institute of Oncology IRCCS, and University of Milan, Milan, Italy. ³⁵The Institute of Cancer Research, London, United Kingdom. ³⁶University of Michigan Rogel Cancer Center, Ann Arbor, MI, USA. *A list of authors and their affiliations appears at the end of the paper. ✉email: balazs.acs@ki.se; david.rimm@yale.edu

Received: 4 February 2022 Revised: 11 April 2022 Accepted: 5 May 2022

Published online: 21 June 2022

INTRODUCTION

It has been long acknowledged that the immunohistochemical (IHC) detection of Ki67 positive tumor cells provides important clinical information in breast cancer¹. More recently, Ki67 gained clinical utility in the T1-2, N0-1, estrogen receptor-positive (ER) and HER2-negative patient group by allowing to identify those patients that are unlikely to benefit from adjuvant chemotherapy². However, Ki67 has not been consistently adopted for clinical care due to unacceptable reproducibility across laboratories³⁻⁵.

Therefore, the International Ki67 in Breast Cancer Working Group (IKWG) originally published consensus recommendations in 2011 for best practices in the application of Ki67 IHC in breast cancer⁶. According to this consensus, parameters that predominantly influence Ki67 IHC results can be grouped into pre-analytical (type of biopsy, tissue handling), analytical (IHC protocol), interpretation and scoring, and data analysis steps⁶. As the scoring method was the largest contributor to test variability⁷, the IKWG has undertaken serious efforts to standardize the Ki67 scoring method of pathologists^{8,9}. Although in multi-institutional studies, standardized Ki67 scoring methods reached pre-defined thresholds for adequate reproducibility^{9,10}, this was only after completing calibration training and by using tedious counting methods. In this context, recently updated guidelines by the IKWG now recommend Ki67 IHC for clinical adoption in specific situations, including the identification of very low (<5) or very high proliferation (>30) indices, that render more expensive gene expression tests unnecessary².

An important additional issue that can cause variability in Ki67 measurements is the type of specimen (core biopsy vs excision) and its effect on Ki67 scoring in a multi-center setting². Indeed, the IKWG recommended use of core biopsies (CB), based on apparent superior results for Ki67 when visual evaluation was compared to that of whole sections (WS).

In this multi-observer and multi-institutional study, we aimed to investigate the comparability of Ki67 measurements across corresponding core biopsy and resection specimens from the same breast cancer cases, when evaluated using a calibrated, automated reading system. Furthermore, we assessed between-(consecutive) section differences in Ki67 scoring as no difference

between sections will facilitate the selection of the tumor-block to perform the IHC staining on.

MATERIALS AND METHODS

Patients

Thirty cases of ER-positive breast cancer used in phase 3 of IKWG initiatives collecting 15 cases from the UK and 15 cases from Japan designed to cover a range of Ki67 scores⁹ were employed in this study. No outcome data were collected for this cohort. Patient selection was irrespective of patients' age at diagnosis, grade, tumor size or lymph node status. The clinicopathological characteristics of these 30 cases can be found in our previous publications^{9,10}.

Tissue preparation and immunohistochemistry (IHC)

Tissues from UK patients, both core biopsies and surgical resections were collected according to ASCO/CAP guidelines, while patients' tissues from Japan were collected following ISO (International Organization for Standardization) 15189 approved by the Japan Accreditation Board. Preparation of the Ki67 slides of the first cohort has been previously described⁹. Briefly, the corresponding core-cut biopsy and surgical resection blocks were centrally cut and stained with Ki67, resulting in 60 Ki67 slides from 30 cases. The IHC was performed using monoclonal antibody MIB-1 at dilution 1:50 (DAKO UK, Cambridgeshire, UK) using an automated staining system (Ventana Medical Systems, Tucson, AZ, USA) according to the consensus criteria established by the International Ki67 Working Group⁶. Sections from the same block were stained in a single immunohistochemistry run, except for four cases where the staining was performed in two different runs. This approach effectively controls for any technical variation in staining.

Sample distribution

Twenty volunteer pathologists from 15 countries, most of whom participated in the previous Phase 3A study, were invited to participate. Four adjacent sections from each of the 60 blocks were centrally stained as follows: the first section with haematoxylin and eosin (H&E), the second with p63 (a myoepithelial marker, to assist the distinction of DCIS from invasive breast cancer) and the third to fourth with Ki67 (designated as slide sets 1-2).

The Aperio ScanScope XT platform was used at 20× magnification to digitize the slides (pixel size: 0.4987 μm × 0.4987 μm), which were uploaded to a server and distributed as digital images. Seventeen pathologists successfully completed the study (Fig. 1).

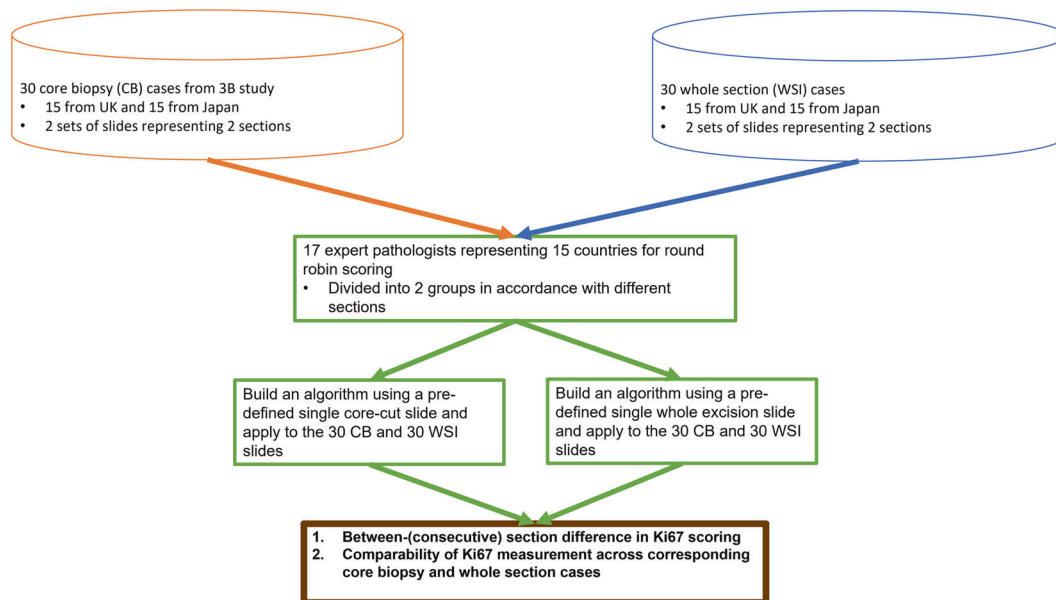


Fig. 1 Study design. Thirty patients of ER-positive breast cancer were enrolled comprising 15 cases from UK and 15 cases from Japan. Corresponding core-cut biopsy and surgical resection blocks were centrally cut two adjacent sections per case and stained with Ki67. Seventeen pathologists from 15 countries were given 60 slides (30 Core cut biopsy slides and 30 surgical resection specimen slides) of Ki67 to score.

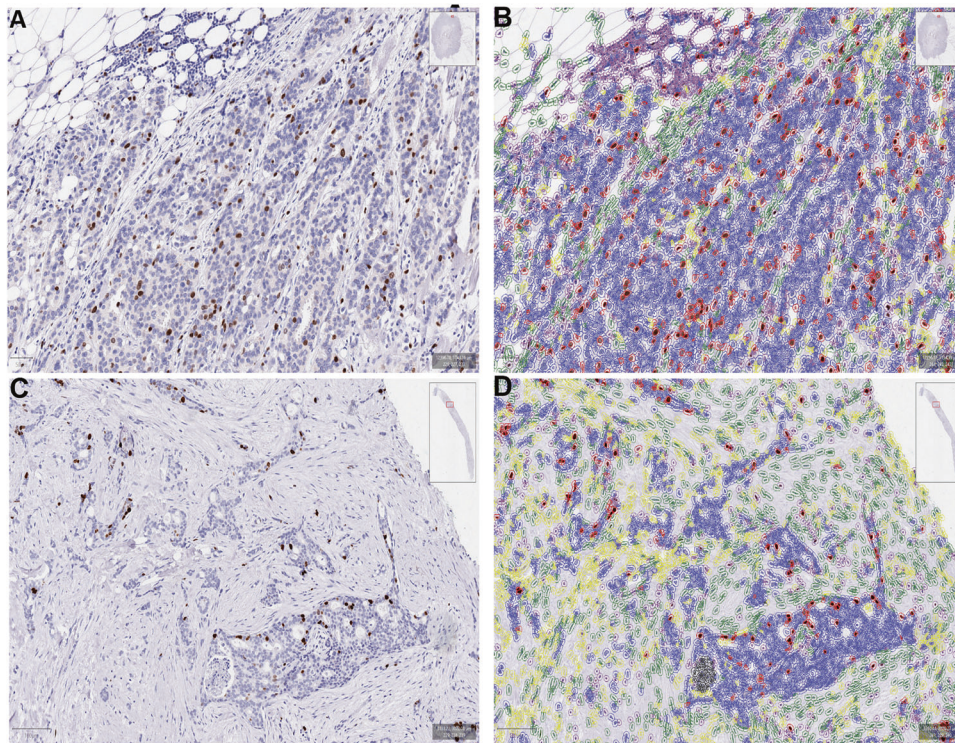


Fig. 2 Digital Image Analysis. Representative pictures of digital image analysis (DIA) masks on a resection specimen (A, B) and a core biopsy case (C, D). Blue corresponds to Ki67 negative tumor cells, red indicates Ki67 positive tumor cells, green indicates stromal cells and purple marks immune cells. Black corresponds to necrosis and yellow marks other detections (false cell detections, noise).

Digital image analysis (DIA)

The QuPath open-source software platform was used to build automated Ki67 scoring algorithms for breast cancer¹¹. A detailed guideline for setting up and building an automated Ki67 scoring algorithm was sent to the participating labs. All the participating labs were requested to build their own Ki67 scoring algorithm following the instructions and apply them on these 60 slides. The complete step by step instructions are available in Supplementary File 1. The reason why we asked each lab to build their own algorithm instead of using the same pre-trained and locked down Ki67 algorithm was to mimic clinical practice. As of the date of the study, no generalizable Ki67 scoring algorithm was available that provides whole slide scoring. Thus, theoretically, all the labs would need to adjust/optimize any such DIA approach to their lab characteristics (different fixation, different antibodies and IHC protocols etc.) necessitating a lab-specific DIA approach. Calibration of the DIA method/guideline was performed in our previous studies demonstrating very good reproducibility among users^{12,13}. Briefly, after the whole invasive cancer area on a digitized slide was annotated, hematoxylin and DAB stain estimates for each case were refined using the “estimate stain vectors” command. We used watershed cell detection¹⁴ to segment the cells in the image with the following settings: Detection image: Optical density sum; requested pixel size: 0.5 μm ; background radius: 8 μm ; median filter radius: 0 μm ; sigma: 1.5 μm ; minimum cell area: 10 μm^2 ; maximum cell area: 400 μm^2 ; threshold: 0.1; maximum background intensity: 2. In order to classify detected cells into tumor cells, immune cells, stromal cells, necrosis and others (false detections, background) (Supplementary File 1), we used random trees as a supervised machine-learning method. The features used in the classification are described in Supplementary Table 1. After setting the optimal color deconvolution and cell segmentation, two independent classifiers were trained on a randomly selected, pre-defined core biopsy (CB classifier) and a resection specimen slide (WSI classifier). Both CB and WSI classifiers were run on both CB slides and resection specimen slides in order to adjust for potentially different characteristics of the two specimen types (Fig. 2).

Statistical analysis

For statistical analysis, SPSS 22 software (IBM, Armonk, USA) software was used. Degree of agreement was evaluated by Bland–Altman plot

and linear regression. To assess differences between specimen type the Wilcoxon signed-rank test was applied, since the data were not normally distributed. Data were visualized using boxplot, spaghetti plot, and dot-plot.

RESULTS

Between-(consecutive) section difference in Ki67 scoring

Very high correlation and no systematic error (bias: -0.6% ; $p = 0.08$) was found between the two consecutive (serial) sections regarding Ki67 scores. If the Ki67 score is higher for a given case, the difference between the sections tends to be also greater (proportional error $p = 0.002$, Fig. 3.), however this difference (0.6% mean difference) does not reach clinical relevance.

Specimen type (CB vs resection specimen) difference in Ki67 scoring

A low correlation was found between core biopsy and whole section excision images (Fig. 4). Ki67 scores were higher when determined on core biopsy slides compared to paired whole sections ($p \leq 0.001$; median difference: 5.31%; IQR: 11.50%) from subsequent surgical excisions of the same tumor. Systematic error occurred between specimens from the same patient as core biopsy Ki67 scores were greater, with a clinically relevant mean difference of 6.6% (bias $p = 0.001$). The limits of agreement also have to be considered wide from a clinical perspective (between -13.7 and 27). Furthermore, Ki67 scores on CB were even higher compared to WS on cases with higher Ki67 scores (proportional error $p = 0.001$). Moreover, the variability of differences in Ki67 scores between CB and WS showed an increasing trend, proportional to the magnitude of Ki67 score (Fig. 4). The same results were found irrespective of the origin of the specimens (CB vs WS $p < 0.001$ for both UK and Japan cases Fig. 5).

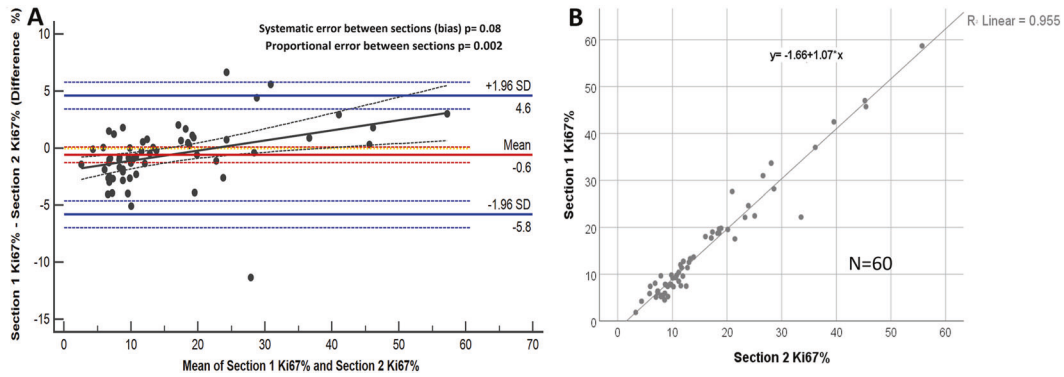


Fig. 3 Between-(consecutive) section difference in Ki67 scoring. Bland–Altman plot comparing Ki67 scores between consecutive sections (A). Orange dashed line corresponds to the expected mean zero difference between Ki67 scores of the two sections. Red line represents the observed mean difference between Ki67 scores of the two sections, namely the observed bias (red dashed lines are the CI of the observed mean difference). Blue lines illustrate the range of agreement (lower and upper limit of agreement) based on 95% of differences (blue dashed lines are the CI of the limits of agreement). Black line is the fitted regression line to detect potential proportional error (black dashed lines are the CI of the regression line). B represents the scatter plot with fitted regression between the Ki67 scores of the two consecutive sections.

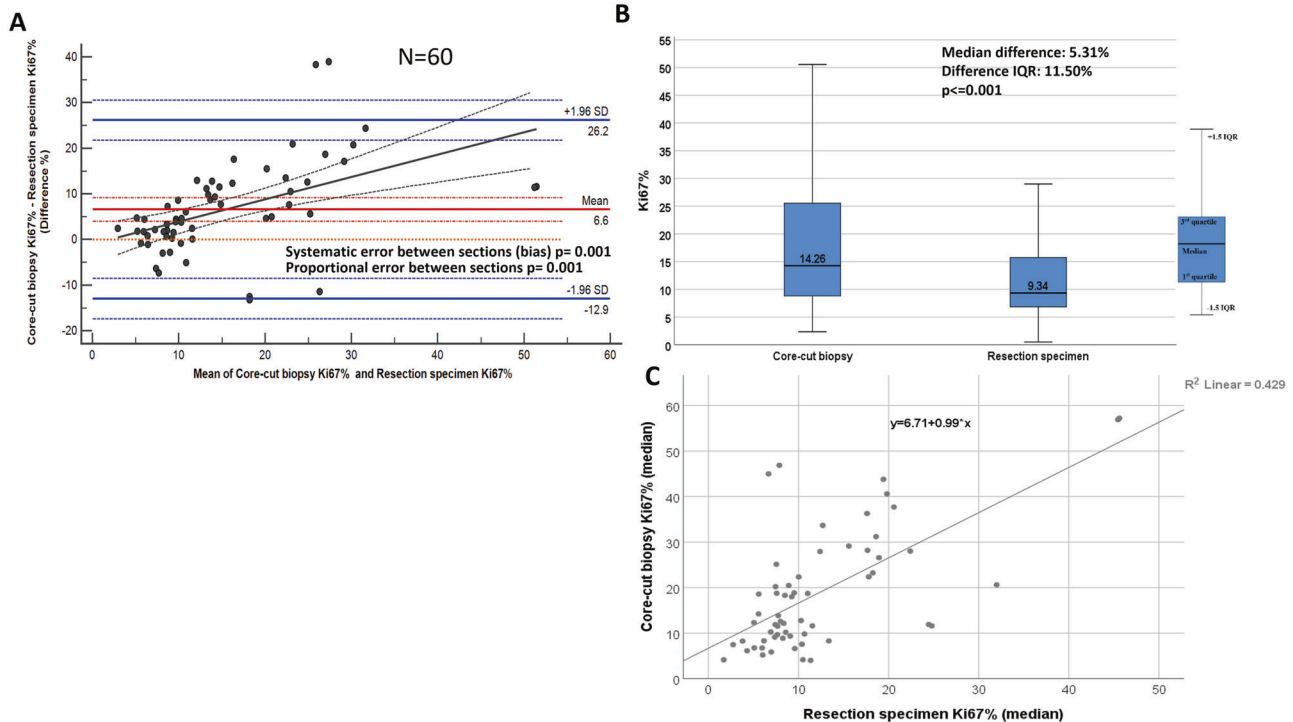


Fig. 4 Between-specimen (CB vs resection specimen) difference in Ki67 scoring. Bland–Altman plot comparing Ki67 scores between specimens (A). Orange dashed line corresponds the expected mean zero difference between Ki67 scores of the two sections. Red line represents the observed mean difference between Ki67 scores of the two sections, namely the observed bias (red dashed lines are the CI of the observed mean difference). Blue lines illustrate the range of agreement (lower and upper limit of agreement) based on 95% of differences (blue dashed lines are the CI of the limits of agreement). Black line is the fitted regression line to detect potential proportional error (black dashed lines are the CI of the regression line). B shows the distributions of Ki67 scores of the two specimens. The bottom/top of the boxes represent the first (Q1)/third (Q3) quartiles, the bold line inside the box represents the median and the two bars outside the box represent the lowest/highest datum still within 1.5x the interquartile range (Q3–Q1). C represents the scatter plot with fitted regression between the Ki67 scores of the two specimens.

DISCUSSION

In this study, we observed that clinically relevant and systematic discrepancies occurred in Ki67 scores between core biopsy and corresponding surgical specimens when evaluated with an automated reading system. Overall, Ki67 scores were higher on CB compared to WS samples. Furthermore, this discrepancy was even more pronounced in tumors that expressed higher levels of Ki67 in general.

Ki67 is one of the most promising yet controversial biomarkers in breast cancer with limited adoption into clinical practice due to its high inter- and intra-laboratory variability^{3,15}. However, Ki67 is widely used in many countries, there is wide variability in its use (to distinguish luminal A-like vs B-like tumors; to determine whether to decide for gene-expression profiling or not; as an adjunct to mitotic counts, etc.), with still no uniformity between clinicians on how to use this biomarker, let alone which cut-off to

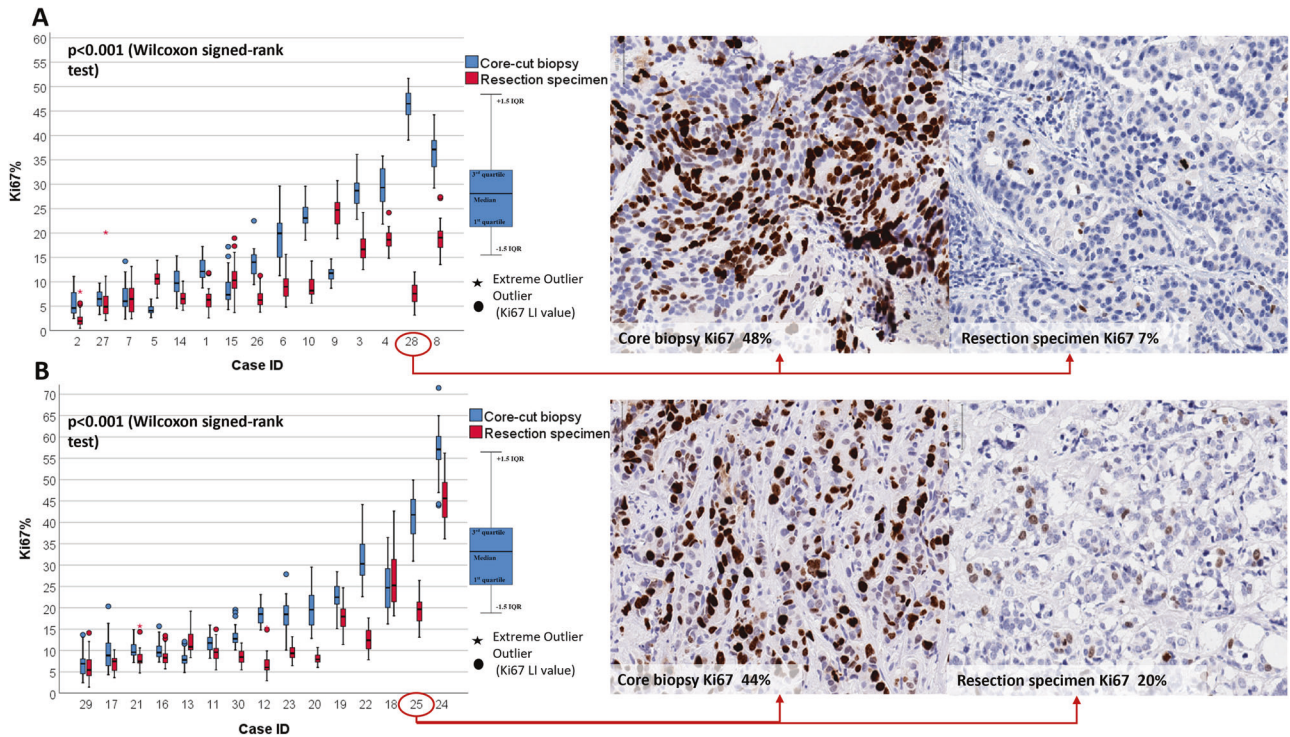


Fig. 5 Between-specimen (CB vs resection specimen) difference in Ki67 scoring by case and by origin of the cases. **A** represents cases collected in the United Kingdom with representative Ki67 IHC images of corresponding CB and resection specimens. **B** represents cases collected in Japan with representative Ki67 IHC images of corresponding CB and resection specimens. The bottom/top of the boxes represent the first (Q1)/third (Q3) quartiles, the bold line inside the box represents the median and the two bars outside the box represent the lowest/highest datum still within 1.5× the interquartile range (Q3–Q1). Outliers are represented with circles, extreme outliers with asterisk.

use. Although the IKWG set up a guideline in 2011 to improve pre-analytical and analytical performance, inter-laboratory protocols still demonstrated low reproducibility related to different sampling, fixation, antigen retrieval, staining and scoring methods^{6,7}. As the latter was the largest single contributor to assay variability, the IKWG has undertaken multi-institution efforts that have standardized visual scoring of Ki67 in a manner which requires on-line calibration tools and careful scoring of several hundred cells, which may or may not be ideal for pathologists in daily practice with time-constraints^{8,9}. This result suggests that digital solutions may still be required to address this issue.

The rise of digital image analysis (DIA) platforms has improved capacity and automation in biomarker evaluation^{16,17}. DIA platforms are able to assess nuclear IHC biomarkers such as Ki67, and numerous studies have been conducted to compare human visual scoring with DIA platforms^{12,18–28}. Although the latest guideline of IKWG recommends Ki67 for clinical practice in specific situations, the type of specimen as a potential pre-analytical factor contributing to Ki67 variability was not specifically investigated in a multi-operator/multi-center setting. In this study we aimed to address these biospecimen questions including assessment by specimen type and between serial sections.

One explanation for our finding would be the presence of tumor heterogeneity, and the broader field of review in a whole section from resection specimen. However, one would expect that this cause of discrepancy would result in random discordance, not the consistent finding that Ki67 scores on core biopsies are higher than that of on resection specimens. Rather, we conclude that lower Ki67 in resection specimens is more easily explained by pre-analytical factors. For example, since longer times to fixation occur with resection specimens compared to CB, persistent cell division will occur even in an unfixed, hypoxic environment. Further, epitope degradation also occurs with prolonged time to fixation^{29–31}.

In addition, one can expect that hot spot scoring might lead to less discrepancy between CB and WS because it considers only the hottest area of Ki67 positivity (highest percentiles of Ki67 distribution) on both specimen types, while global assessment evaluates the total Ki67 distribution which can be variable¹⁰. However, there remains a fundamental issue of exact hot spot definition and where pathologists set its boundaries. Moreover, the International Ki67 Working Group has recommended global scoring over hot spot as it did show a consistent trend towards increased reproducibility in both core biopsy⁹ and excision¹⁰ specimens.

Additional support for the conclusion that the difference in Ki67 between CB and WS is provided by the observation of clinically relevant differences between specimens in cases from different institutions used in this study, independently scored multiple times by 17 pathologists. Although many studies focused on assessing the level of agreement between CB and resection samples in Ki67 scoring; consensus was not possible due to lack of standardization³².

Our results are consistent with previous results showing poor/moderate concordance ($\kappa = 0.195–0.814$) occurring between CB and resection specimen in Ki67 scoring^{1,33–46}. However, some studies showed higher Ki67 scores on resection samples^{35,36,38}. This discrepancy among studies may be due to lack of standardization in methodology leading to different scoring methods, which we have previously demonstrated to be highly variable². Moreover, inter-institutional discrepancies could also be the result of different antibodies and protocols used to detect Ki67, different tissue handling/fixation protocols and at some point tumor Ki67 heterogeneity since Ki67 is heterogeneous in tumors⁶. Thus, our findings provide further support to the latest IKWG recommendations and provide a consensus that Ki67 should be ideally tested on CB samples because it minimizes many fixation problems as Ki67 IHC is more sensitive than ER or HER2 to

variabilities in fixation². Since pre-analytical factors are critical in diagnostic pathology, the IKWG recommends that breast cancer samples for Ki67 testing should be processed in line with ASCO/CAP guidelines².

There are a number of limitations in this study. This study only focused on analytical and preanalytical questions, therefore we cannot demonstrate the clinical validation of the calibrated tool. There are many other studies that address the prognostic or predictive value of this test, and that goal was beyond the scope of this effort. For the same reason, further clinical studies are needed to demonstrate how does this consistent difference in Ki67 between corresponding core-cuts and resection specimen impact on prognostic value or its clinical implication on the assessment of neoadjuvant endocrine therapy benefit. Furthermore, the low correlation suggests a critical difference between a core biopsy score and a whole section excision score, which can undermine the use of data on outcome, derived predominantly from resection samples, to identify patients at high risk using a score derived from a core biopsy. Therefore, this study suggests caution in this approach given that even without intervening therapy a clinically relevant change in Ki67 may occur. Further, the Ki67 assessments were based on biospecimens from only 2 central sites. While the participating pathologists within the IKWG represented 15 countries, specimens were centrally acquired and stained. Whereas other investigators have compared specimens from multiple different sites^{5,7,47} we limited the number of sites to remove the variables associated with the technical aspect of the stain. Finally, while the core cut biopsy and resection are from the same case, only a single core was assessed. Thus, we could be missing heterogeneity seen in larger resection specimens. The effect of heterogeneity could be decreased by taking multiple core cuts when clinical situation allows. However, since examination of a single core cut represents the clinical standard of care in several countries, we did not pursue multiple cores.

In conclusion, while we find no significant difference in digitally-assessed Ki67 index between serial sections, we do find a systematic discrepancy between core biopsy and corresponding whole sections – core biopsy samples yield higher scores (likely due to pre-analytical factors including more standard and prompt tissue handling, fixation, etc.). Therefore, this work suggests that Ki67 IHC tested on core biopsy samples should be preferred to excision specimens in clinical decision-making, because doing so will preclude many pre-analytical factors.

DATA AVAILABILITY

The datasets used and/or analyzed during the current study are available from the corresponding author on reasonable request.

REFERENCES

- Smith I, Robertson J, Kilburn L, Wilcox M, Evans A, Holcombe C, et al. Long-term outcome and prognostic value of Ki67 after perioperative endocrine therapy in postmenopausal women with hormone-sensitive early breast cancer (POETIC): an open-label multicentre parallel-group randomised phase 3 trial. *Lancet Oncol* 21, 1443–1454 (2020)
- Nielsen TO, Leung SCY, Rimm DL, Dodson A, Acs B, Badve S, et al. Assessment of Ki67 in breast cancer: updated recommendations from the International Ki67 in Breast Cancer Working Group. *J Natl Cancer Inst* 113, 808–819 (2020)
- Harris LN, Ismaila N, McShane LM, Andre F, Collyar DE, Gonzalez-Angulo AM, et al. Use of biomarkers to guide decisions on adjuvant systemic therapy for women with early-stage invasive breast cancer: American Society of Clinical Oncology Clinical Practice Guideline. *J Clin Oncol* 34, 1134–1150 (2016)
- Andre F, Ismaila N, Henry NL, Somerfield MR, Bast RC, Barlow W, et al. Use of biomarkers to guide decisions on adjuvant systemic therapy for women with early-stage invasive breast cancer: ASCO Clinical Practice Guideline Update-Integration of Results From TAILORx. *J Clin Oncol* 37, 1956–1964 (2019)
- Acs B, Fredriksson I, Rönnlund C, Hagerling C, Ehinger A, Kovács A, et al. Variability in breast cancer biomarker assessment and the effect on oncological

- treatment decisions: a nationwide 5-year population-based study. *Cancers (Basel)* 13, 1166 (2021)
- Dowsett M, Nielsen TO, A'Hern R, Bartlett J, Coombes RC, Cuzick J, et al. Assessment of ki67 in breast cancer: recommendations from the international ki67 in breast cancer working group. *J Natl Cancer Inst* 103, 1656–1664 (2011)
 - Polley MY, Leung SC, McShane LM, Gao D, Hugh JC, Mastropasqua MG, et al. An international Ki67 reproducibility study. *J Natl Cancer Inst* 105, 1897–1906 (2013)
 - Polley MY, Leung SC, Gao D, Mastropasqua MG, Zabaglo LA, Bartlett JM, et al. An international study to increase concordance in Ki67 scoring. *Mod Pathol* 28, 778–786 (2015)
 - Leung SCY, Nielsen TO, Zabaglo L, Arun I, Badve SS, Bane AL, et al. Analytical validation of a standardized scoring protocol for Ki67: phase 3 of an international multicenter collaboration. *NPJ Breast Cancer* 2, 16014 (2016)
 - Leung SCY, Nielsen TO, Zabaglo LA, Arun I, Badve SS, Bane AL, et al. Analytical validation of a standardised scoring protocol for Ki67 immunohistochemistry on breast cancer excision whole sections: an international multicentre collaboration. *Histopathology* 75, 225–235 (2019)
 - Bankhead P, Loughrey MB, Fernandez JA, Dombrowski Y, McArt DG, Dunne PD, et al. QuPath: Open source software for digital pathology image analysis. *Sci Rep* 7, 16878 (2017)
 - Acs B, Pelekanou V, Bai Y, Martinez-Morilla S, Toki M, Leung SCY, et al. Ki67 reproducibility using digital image analysis: an inter-platform and inter-operator study. *Lab Invest* 99, 107–117 (2019)
 - Aung TN, Acs B, Warrell J, Bai Y, Gaule P, Martinez-Morilla S, et al. A new tool for technical standardization of the Ki67 immunohistochemical assay. *Mod Pathol* 34, 1261–1270 (2021)
 - Malpica N, de Solorzano CO, Vaquero JJ, Santos A, Vallcorba I, Garcia-Sagredo JM, et al. Applying watershed algorithms to the segmentation of clustered nuclei. *Cytometry* 28, 289–297 (1997)
 - Kos Z, Dabbs DJ. Biomarker assessment and molecular testing for prognostication in breast cancer. *Histopathology* 68, 70–85 (2016)
 - Kayser K, Gortler J, Borckenfeld S, Kayser G. How to measure diagnosis-associated information in virtual slides. *Diagn Pathol* 6, Suppl 1 S9 (2011)
 - Robertson S, Azizpour H, Smith K, Hartman J. Digital image analysis in breast pathology-from image processing techniques to artificial intelligence. *Transl Res* 194, 19–35 (2018)
 - Wienert S, Heim D, Kotani M, Lindequist B, Stenzinger A, Ishii M, et al. CognitionMaster: an object-based image analysis framework. *Diagn Pathol* 8, 34 (2013)
 - Laurinavicius A, Plancoulaine B, Laurinaviciene A, Herlin P, Meskauskas R, Baltrusaityte I, et al. A methodology to ensure and improve accuracy of Ki67 labelling index estimation by automated digital image analysis in breast cancer tissue. *Breast Cancer Res* 16, R35 (2014)
 - Klauschen F, Wienert S, Schmitt WD, Loibl S, Gerber B, Blohmer JU, et al. Standardized Ki67 diagnostics using automated scoring-clinical validation in the gepartrio breast cancer study. *Clin Cancer Res* 21, 3651–3657 (2015)
 - Stalhammar G, Fuentes Martinez N, Lippert M, Tobin N,P Molholm I, Kis L, et al. Digital image analysis outperforms manual biomarker assessment in breast cancer. *Mod Pathol* 29, 318–329 (2016)
 - Acs B, Madaras L, Kovacs KA, Micsik T, Tokes AM, Gyorffy B, et al. Reproducibility and prognostic potential of Ki-67 proliferation index when comparing digital-image analysis with standard semi-quantitative evaluation in breast cancer. *Pathol Oncol Res* 24, 115–127 (2018)
 - Zhong F, Bi R, Yu B, Yang F, Yang W, Shui R. A comparison of visual assessment and automated digital image analysis of Ki67 labeling index in breast cancer. *PLoS One* 11, e0150505 (2016)
 - Stalhammar G, Robertson S, Wedlund L, Lippert M, Rantalainen M, Bergh J, et al. Digital image analysis of Ki67 in hot spots is superior to both manual Ki67 and mitotic counts in breast cancer. *Histopathology* 72, 974–989 (2018)
 - Rimm DL, Leung SCY, McShane LM, Bai Y, Bane AL, Bartlett JMS, et al. An international multicenter study to evaluate reproducibility of automated scoring for assessment of Ki67 in breast cancer. *Mod Pathol* 32, 59–69 (2019)
 - Robertson S, Acs B, Lippert M, Hartman J. Prognostic potential of automated Ki67 evaluation in breast cancer: different hot spot definitions versus true global score. *Breast Cancer Res Treat* 183, 161–175 (2020)
 - Koopman T, Buikema HJ, Hollema H, de Bock GH, van der Vegt B. Digital image analysis of Ki67 proliferation index in breast cancer using virtual dual staining on whole tissue sections: clinical validation and inter-platform agreement. *Breast Cancer Res Treat* 169, 33–42 (2018)
 - Plancoulaine B, Laurinaviciene A, Herlin P, Besusparis J, Meskauskas R, Baltrusaityte I, et al. A methodology for comprehensive breast cancer Ki67 labeling index with intra-tumor heterogeneity appraisal based on hexagonal tiling of digital image analysis data. *Virchows Arch* 467, 711–722 (2015)
 - Arima N, Nishimura R, Osako T, Nishiyama Y, Fujisue M, Okumura Y, et al. The importance of tissue handling of surgically removed breast cancer for an accurate assessment of the Ki-67 index. *J Clin Pathol* 69, 255–259 (2016)

30. Mengel M, von Wasielewski R, Wiese B, Rüdiger T, Müller-Hermelink HK, Kreipe H. Inter-laboratory and inter-observer reproducibility of immunohistochemical assessment of the Ki-67 labelling index in a large multi-centre trial. *J Pathol* 198, 292–299 (2002)
31. Benini E, Rao S, Daidone MG, Pilotti S, Silvestrini R. Immunoreactivity to MIB-1 in breast cancer: methodological assessment and comparison with other proliferation indices. *Cell Prolif* 30, 107–115 (1997)
32. Kalvala J, Parks RM, Green AR, Cheung KL. Concordance between core needle biopsy and surgical excision specimens for Ki-67 in breast cancer - a systematic review of the literature. *Histopathology* 80, 468–484 (2022)
33. Janeva S, Parris TZ, Nasic S, De Lara S, Larsson K, Audisio RA, et al. Comparison of breast cancer surrogate subtyping using a closed-system RT-qPCR breast cancer assay and immunohistochemistry on 100 core needle biopsies with matching surgical specimens. *BMC Cancer* 21, 439 (2021).
34. Greer LT, Rosman M, Mylander WC, Hooke J, Kovatic A, Sawyer K, et al. Does breast tumor heterogeneity necessitate further immunohistochemical staining on surgical specimens? *J Am Coll Surg* 216, 239–251 (2013)
35. Chen X, Sun L, Mao Y, Zhu S, Wu J, Huang O, et al. Preoperative core needle biopsy is accurate in determining molecular subtypes in invasive breast cancer. *BMC Cancer* 13, 390 (2013)
36. Chen X, Zhu S, Fei X, Garfield DH, Wu J, Huang O, et al. Surgery time interval and molecular subtype may influence Ki67 change after core needle biopsy in breast cancer patients. *BMC Cancer* 15, 822 (2015)
37. Kalkman S, Bulte JP, Halilovic, A Bult P, van Diest PJ. Brief fixation does not hamper the reliability of Ki67 analysis in breast cancer core-needle biopsies: a double-centre study. *Histopathology* 66, 380–387 (2015)
38. Al Nemer A. The performance of Ki-67 labeling index in different specimen categories of invasive ductal carcinoma of the breast using 2 scoring methods. *Appl Immunohistochem Mol Morphol* 25, 86–90 (2017)
39. Pölcher M, Braun M, Tischitz M, Hamann M, Szeterlak N, Kriegmair A, et al. Concordance of the molecular subtype classification between core needle biopsy and surgical specimen in primary breast cancer. *Arch Gynecol Obstet* 304, 783–790 (2021)
40. Liu M, Tang SX, Tsang JYS, Shi YJ, Ni YB, Law BKB, et al. Core needle biopsy as an alternative to whole section in IHC4 score assessment for breast cancer prognostication. *J Clin Pathol* 71, 1084–1089 (2018)
41. You K, Park S, Ryu JM, Kim I, Lee SK, Yu J, et al. Comparison of core needle biopsy and surgical specimens in determining intrinsic biological subtypes of breast cancer with immunohistochemistry. *J Breast Cancer* 20, 297–303 (2017)
42. Chen J, Wang Z, Lv Q, Du Z, Tan Q, Zhang D, et al. Comparison of core needle biopsy and excision specimens for the accurate evaluation of breast cancer molecular markers: a report of 1003 cases. *Pathol Oncol Res* 23, 769–775 (2017)
43. Focke CM, Decker T, van Diest PJ. Reliability of the Ki67-labelling index in core needle biopsies of luminal breast cancers is unaffected by biopsy volume. *Ann Surg Oncol* 24, 1251–1257 (2017)
44. Meattini I, Bicchierai G, Saieva C, De Benedetto D, Desideri I, Becherini C, et al. Impact of molecular subtypes classification concordance between preoperative core needle biopsy and surgical specimen on early breast cancer management: Single-institution experience and review of published literature. *Eur J Surg Oncol* 43, 642–648 (2017)
45. Robertson S, Rönnlund C, de Boniface J, Hartman J. Re-testing of predictive biomarkers on surgical breast cancer specimens is clinically relevant. *Breast Cancer Res Treat* 174, 795–805 (2019)
46. Clark BZ, Onisko A, Assylbekova B, Li X, Bhargava R, Dabbs DJ. Breast cancer global tumor biomarkers: a quality assurance study of intratumoral heterogeneity. *Mod Pathol* 32, 354–366 (2019)
47. Ekholm M, Grabau D, Bendahl PO, Bergh J, Elmberger G, Olsson H, et al. Highly reproducible results of breast cancer biomarkers when analysed in accordance with national guidelines - a Swedish survey with central re-assessment. *Acta Oncol* 54, 1040–1048 (2015)

ACKNOWLEDGEMENTS

We are grateful to the Breast International Group and North American Breast Cancer Group (BIG-NABCG) collaboration, including the leadership of Nancy Davidson, Thomas Buchholz, Martine Piccart, and Larry Norton.

AUTHOR CONTRIBUTIONS

BA, DLR, SCYL, TON, DFH and MD performed study concept and design; BA, DLR, SCYL performed development of methodology. All authors except DLR, TON, DFH, MD provided analysis, data acquisition and data curation. BA, SCYL, KMK provided statistical analysis. BA, DLR, SCYL, TON, DFH, MD, KMK provided interpretation of data.

BA, DLR, SCYL, TON, DFH, MD wrote the first draft of the paper. All authors provided review, revision of the manuscript and approved the final paper.

FUNDING

BA is supported by The Swedish Society for Medical Research (Svenska Sällskapet för Medicinsk Forskning) Postdoctoral grant, Swedish Breast Cancer Association (Bröstcancerförbundet) Research grant 2021, The Fulbright Program and The Rosztoczy Foundation Scholarship Program. MD, DFH, RS (BCRF grant N° 17–194), (many others) and DLR are supported by the Breast Cancer Research Foundation. This work was supported by a generous grant from the Breast Cancer Research Foundation (DFH). Additional funding for the UK laboratories was received from Breakthrough Breast Cancer and the National Institute for Health Research Biomedical Research Centre at the Royal Marsden Hospital. Funding for the Ontario Institute for Cancer Research is provided by the Government of Ontario. JH is the Lilian McCullough Chair in Breast Cancer Surgery Research and the CBCF Prairies/NWT Chapter. Open access funding provided by Karolinska Institute.

COMPETING INTERESTS

In the last 12 months, DLR has served as a consultant for advisor to Astra Zeneca, Agendia, Amgen, Cell Signaling Technology, Cepheid, Danaher, Konica-Minolta, Merck, PAIGE.AI, Regeneron, and Sanofi. TON reports a proprietary interest in PAM50/Prosigna and consultant work with Veracyte. JH was former member of the advisory board at Visiopharm A/S. JH has obtained speaker's honoraria or advisory board remunerations from Roche, Novartis, AstraZeneca, Eli Lilly, Pfizer and MSD. JH is co-founder and shareholder of Stratipath AB. JH has received institutional research grants from Cepheid and Novartis. DFH reports no research or personal financial support related to this study. DFH does report research support unrelated to this study provided to his institution during conduct from Menarini/Silicon BioSystems, Astra Zeneca, Eli Lilly Company, Merrimack Pharmaceuticals, Inc. (Parexel Intl Corp), Veridex and Janssen Diagnostics (Johnson & Johnson), Pfizer, and Puma Biotechnology, Inc. (subcontract Wash Univ St. Louis to Univ Mich). DFH also reports that his institution holds a patent regarding circulating tumor cell characterization for which DFH is the named investigator that was licensed to Menarini Silicon Biosystems and from which both received annual royalties, ending in January 2021. DFH reports personal income related to consulting or advisory board activities from BioVeca, Cellworks, Cepheid, EPIC Sciences, Freenome, Guardant, L-Nutra, Oncocyte, MacroGenics, Predictus BioSciences, Salutogenic Innovations, Turnstone Biologics, and Tempus. DFH reports personally held stock options from InBiomotion. BvdV reports speaker's honoraria or consultation/advisory board remunerations provided to his institution from Visiopharm, Philips, Merck/MSD and DiaCeutics. GV reports receipt of grants/research supports from Roche/Genentech, Ventana Silicon Systems, Dako/Agilent Technologies, and receipt of honoraria or consultation fees from Ventana, Dako/Agilent, Roche, MSD Oncology, AstraZeneca, Daiichi Sankyo, Pfizer, Eli Lilly. ZK has served in a paid advisory role to Eli Lilly. Unrelated to this study, SR is currently employed by Stratipath AB. RS reports non-financial support from Merck and Bristol Myers Squibb; research support from Merck, Puma Biotechnology, and Roche; and advisory board fees for Bristol Myers Squibb; and personal fees from Roche for an advisory board related to a trial-research project. RS has no COI related to this project. SF served as expert pathology consultant for Axdev Global Corp inc and as an expert advisory panel for Genomic Health in 2017. RML is co-founder and shareholder of MUSE Microscopy, Inc. and Histolix, Inc. RML served as consultant for Cell IDx, Inc., BriteSeed, Inc., ImmunoPhotonics, Inc., Pathology Watch, Inc. and Verily, Inc. FPL reports board meetings and conference support from Astrazeneca, Lilly, Novartis, Pfizer and Roche. JB served as consultant for Insight Genetics, Inc., BioNTech AG, Biotheranostics, Inc., Pfizer, Rna Diagnostics Inc., oncoXchange/MedcomXchange Communications Inc, Herbert Smith French Solicitors, OncoCyte Corporation. JB served as member of the scientific advisory board for MedcomXchange Communications Inc. JB reports honoraria from NanoString Technologies, Inc., Oncology Education, Biotheranostics, Inc., MedcomXchange Communications Inc. JB reports travel and accommodation expenses support from Biotheranostics, Inc., NanoString Technologies, Inc., Breast Cancer Society of Canada. JB received research funding from Thermo Fisher Scientific, Genoptix, Agendia, NanoString Technologies, Inc., Stratifyer GmbH, Biotheranostics, Inc. The remaining authors declare no competing interests.

ETHICS APPROVAL AND CONSENT TO PARTICIPATE

The study was approved by the British Columbia Cancer Agency's Clinical Research Ethics Board (H10-03420).

ADDITIONAL INFORMATION

Supplementary information The online version contains supplementary material available at <https://doi.org/10.1038/s41379-022-01104-9>.

Correspondence and requests for materials should be addressed to Balazs Acs or David L. Rimm.

Reprints and permission information is available at <http://www.nature.com/reprints>

Publisher's note Springer Nature remains neutral with regard to jurisdictional claims in published maps and institutional affiliations.



Open Access This article is licensed under a Creative Commons Attribution 4.0 International License, which permits use, sharing, adaptation, distribution and reproduction in any medium or format, as long as you give appropriate credit to the original author(s) and the source, provide a link to the Creative Commons license, and indicate if changes were made. The images or other third party material in this article are included in the article's Creative Commons license, unless indicated otherwise in a credit line to the material. If material is not included in the article's Creative Commons license and your intended use is not permitted by statutory regulation or exceeds the permitted use, you will need to obtain permission directly from the copyright holder. To view a copy of this license, visit <http://creativecommons.org/licenses/by/4.0/>.

© The Author(s) 2022

ON BEHALF OF THE INTERNATIONAL KI67 IN BREAST CANCER WORKING GROUP OF THE BREAST INTERNATIONAL GROUP AND NORTH AMERICAN BREAST CANCER GROUP (BIG-NABCG)

Mitch Dowsett³⁷, Daniel F. Hayes³⁸, Lisa M. McShane³⁹, Kelley M. Kidwell⁴⁰, Torsten Nielsen⁴¹, Samuel Leung⁴¹, Balazs Acs⁴², Indu Arun⁴³, Renaldas Augulis⁴⁴, Sunil S. Badve⁴⁵, Yalai Bai⁴⁶, Anita L. Bane⁴⁷, John M. S. Bartlett⁴⁸, Jane Bayani⁴⁸, Gilbert Bigras⁴⁹, Annika Blank⁵⁰, Signe Borgquist⁵¹, Henk Buikema⁵², Angela Chan⁵³, Martin C. Chang⁵⁴, Carsten Denkert⁵⁵, Robin L. Dietz⁵⁶, Andrew Dodson⁵⁷, Anna Ehinger⁵¹, Matthew Ellis⁵⁸, Susan Fineberg⁵⁹, Margaret Flowers⁶⁰, Cornelia M. Focke⁶¹, Chad Galderisi⁶², Dongxia Gao⁶³, Abhi Gholap⁶⁴, Allen M. Gown⁶⁵, Carolina Gutierrez⁶⁶, Douglas J. Hartman⁶⁷, Johan Hartman⁶⁸, Judith C. Hugh⁴⁹, Anagha Jadhav⁶⁴, Elizabeth N. Kornaga⁶⁹, Zuzana Kos⁷⁰, Hans Kreipe⁷¹, Anne-Vibeke Lænkholm⁷², Arvydas Laurinavicius⁴⁴, Richard Levenson⁷³, Mauro Mastropasqua⁷⁴, Takuya Moriya⁷⁵, Sharon Nofech-Mozes⁷⁶, C. Kent Osborne⁶⁶, Hongchao Pan⁷⁷, Liron Pantanowitz⁷⁸, Ernesta Paola Neri⁷⁹, Frédérique M. Penault-Llorca⁸⁰, Mei-Yin Polley⁸¹, Tammy Piper⁸², Mary Anne Quintayo⁸³, Tilman T. Rau⁸⁴, David L. Rimm⁴⁶, Stefan Reinhard⁸⁵, Stephanie Robertson⁶⁸, Jason Ruan⁷³, Takashi Sakatani⁸⁶, Roberto Salgado⁸⁷, Lois Shepherd⁸⁸, Ian Smith⁸⁹, Joseph Sparano⁵⁹, Melanie Spears⁴⁸, Malini Srinivasan⁶⁷, Jane Starczynski⁹⁰, Tomoharu Sugie⁹¹, Austin Todd⁷³, Bert van der Vegt⁵², Giuseppe Viale⁹², Shakeel Virk⁹³, Yihong Wang⁹⁴, Hua Yang⁵³, Lila A. Zabaglo⁹⁵, Zhiwei Zhang⁹⁶ and Inti Zlobec⁸⁵

³⁷Academic Department of Biochemistry, Royal Marsden Hospital / Institute of Cancer Research, London, UK. ³⁸Breast Oncology Program, Department of Internal Medicine, University of Michigan Comprehensive Cancer Center, Ann Arbor, MI, USA. ³⁹National Cancer Institute, Bethesda, MD, USA. ⁴⁰Department of Biostatistics, School of Public Health, University of Michigan, Ann Arbor, MI, USA. ⁴¹Genetic Pathology Evaluation Centre, Department of Pathology and Laboratory Medicine, University of British Columbia, Vancouver, BC, Canada. ⁴²Karolinska Institutet, Stockholm, Sweden. ⁴³Tata Medical Center, Kolkata, West Bengal, India. ⁴⁴Vilnius University Hospital Santara Clinics, Vilnius University, Vilnius, Lithuania. ⁴⁵Indiana University Simon Cancer Center, Indianapolis, IN, USA. ⁴⁶Yale University School of Medicine, New Haven, CT, USA. ⁴⁷Juravinski Hospital and Cancer Centre, McMaster University, Hamilton, ON, Canada. ⁴⁸Ontario Institute for Cancer Research, Toronto, ON, Canada. ⁴⁹University of Alberta, Edmonton, AB, Canada. ⁵⁰Institute of Pathology, Triemli Hospital Zurich, Zurich, Switzerland. ⁵¹Skane University Hospital, Lund University, Lund, Sweden. ⁵²University Medical Center Groningen, Groningen, The Netherlands. ⁵³Department of Laboratory Medicine and Pathology, University of Alberta, Edmonton, AB, Canada. ⁵⁴Department of Pathology & Laboratory Medicine, University of Vermont Medical Center, Burlington, VT, USA. ⁵⁵Charité Campus Mitte, Berlin, Germany. ⁵⁶Department of Pathology, University of Pittsburgh, Pittsburgh, PA, USA. ⁵⁷UK NEQAS for Immunocytochemistry and In-Situ Hybridisation, London, UK. ⁵⁸Baylor College of Medicine, Houston, TX, USA. ⁵⁹Montefiore Medical Center and the Albert Einstein College of Medicine, Bronx, NY, USA. ⁶⁰Breast Cancer Research Foundation, New York, NY, USA. ⁶¹Dietrich-Bonhoeffer Medical Center, Neubrandenburg, Mecklenburg-Vorpommern, Germany. ⁶²MolecularMD, Portland, OR, USA. ⁶³University of British Columbia, Vancouver, BC, Canada. ⁶⁴Optra Technologies, NeoPro SEZ, BlueRidge, Hinjewadi, India. ⁶⁵Department of Pathology and Laboratory Medicine, University of British Columbia, Vancouver, BC, Canada. ⁶⁶Lester and Sue Smith Breast Center and Dan L. Duncan Comprehensive Cancer Center, Baylor College of Medicine, Houston, TX, USA. ⁶⁷University of Pittsburgh, Pittsburgh, PA, USA. ⁶⁸Department of Oncology-Pathology, Karolinska Institutet, Stockholm, Sweden. ⁶⁹Tom Baker Cancer Centre, Alberta Health Services, Calgary, AB, Canada. ⁷⁰BC Cancer, Vancouver, BC, Canada. ⁷¹Medical School Hannover, Institute of Pathology, Hannover, Germany. ⁷²Zealand University Hospital, Slagelse, Region Sjælland, Denmark. ⁷³University of California Davis Medical Center, Sacramento, CA, USA. ⁷⁴European Institute of Oncology, Milan, Italy. ⁷⁵Kawasaki Medical School, Kurashiki, Okayama Prefecture, Japan. ⁷⁶University of Toronto Sunnybrook Health Sciences Centre, Toronto, ON, Canada. ⁷⁷Nuffield Department of Population Health, University of Oxford, Oxford, UK. ⁷⁸Department of Pathology & Clinical Labs, University of Michigan, Ann Arbor, MI, USA. ⁷⁹Translational Laboratories, Tom Baker Cancer Centre, Alberta Health Services, Calgary, AB, Canada. ⁸⁰Centre Jean Perrin and Université d'Auvergne, Clermont-Ferrand, France. ⁸¹Department of Public Health Sciences, The University of Chicago Biological Sciences, Chicago, IL, USA. ⁸²Edinburgh Cancer Research Centre, Western General Hospital, Edinburgh, United Kingdom. ⁸³Transformative Pathology, Ontario Institute for Cancer Research, Toronto, ON, Canada. ⁸⁴Institute of Pathology, Heinrich Heine University and University Hospital of Duesseldorf, Duesseldorf, Germany. ⁸⁵Universität Bern Institut für Pathologie, Murtenstrasse, Bern, Switzerland. ⁸⁶Nippon Medical School, Bunkyo-ku, Tokyo, Japan. ⁸⁷Institut Jules Bordet, Brussels, Belgium. ⁸⁸Department of Pathology and Molecular Medicine, Queen's University, Kingston, ON, Canada. ⁸⁹Ralph Lauren Centre for Breast Cancer Research, The Royal Marsden Hospital, London, United Kingdom. ⁹⁰Birmingham Heart of England, National Health Service, Birmingham, United Kingdom. ⁹¹Kansai Medical University, Hirakata, Osaka, Japan. ⁹²University of Milan, Milan, Italy. ⁹³Queen's University, Kingston, ON, Canada. ⁹⁴Rhode Island Hospital, Brown University, Providence, RI, USA. ⁹⁵The Institute of Cancer Research, London, United Kingdom. ⁹⁶Biometric Research Program, Division of Cancer Treatment and Diagnosis, National Cancer Institute, Bethesda, MD, USA.

ARTICLE OPEN



Interplay between copy number alterations and immune profiles in the early breast cancer Scandinavian Breast Group 2004-1 randomized phase II trial: results from a feasibility study

Ioannis Zerdas ^{1,2,8}, Michele Simonetti ^{3,4,8}, Alexios Matikas ^{1,2,8}, Luuk Harbers ^{3,4}, Balazs Acs ^{1,5}, Ceren Boyaci ^{1,5}, Ning Zhang ^{3,4}, Dimitrios Salgkakis ¹, Susanne Agartz ¹, Pablo Moreno-Ruiz ¹, Yalai Bai ⁶, David L. Rimm ⁶, Johan Hartman ^{1,5}, Artur Mezheyski ⁷, Jonas Bergh ^{1,2,9}✉, Nicola Crosetto ^{3,4,9}✉ and Theodoros Foukakis ^{1,2,9}✉

Emerging data indicate that genomic alterations can shape immune cell composition in early breast cancer. However, there is a need for complementary imaging and sequencing methods for the quantitative assessment of combined somatic copy number alteration (SCNA) and immune profiling in pathological samples. Here, we tested the feasibility of three approaches—CUTseq, for high-throughput low-input SCNA profiling, multiplexed fluorescent immunohistochemistry (mFHC) and digital-image analysis (DIA) for quantitative immuno-profiling— in archival formalin-fixed paraffin-embedded (FFPE) tissue samples from patients enrolled in the randomized SBG-2004-1 phase II trial. CUTseq was able to reproducibly identify amplification and deletion events with a resolution of 100 kb using only 6 ng of DNA extracted from FFPE tissue and pooling together 77 samples into the same sequencing library. In the same samples, mFHC revealed that CD4 + T-cells and CD68 + macrophages were the most abundant immune cells and they mostly expressed PD-L1 and PD-1. Combined analysis showed that the SCNA burden was inversely associated with lymphocytic infiltration. Our results set the basis for further applications of CUTseq, mFHC and DIA to larger cohorts of early breast cancer patients.

npj Breast Cancer (2021)7:144; <https://doi.org/10.1038/s41523-021-00352-3>

INTRODUCTION

The substantial proportion of patients with breast cancer (BC) that do not respond to immunotherapy by checkpoint inhibition underscores the importance of identifying reliable predictive biomarkers. To date, the only prospectively validated marker remains Programmed Death Ligand 1 (PD-L1) protein expression, which predicts benefit to immunotherapy in metastatic triple-negative BC, albeit with contradictory results depending on the chemotherapy backbone^{1,2}. Moreover, PD-L1 protein detection has been characterized by controversial analytical performance and ambiguous prognostic role in BC³. Other factors that describe or determine tumor-host interactions such as tumor-infiltrating lymphocytes (TILs), gene expression immune signatures and tumor mutational burden (TMB) represent markers of response to chemotherapy^{4–7}, with emerging data also supporting prediction of benefit from immunotherapy^{8,9}. Furthermore, genome instability, aneuploidy, as well as immune evasion have been recognized as important biomarkers of BC progression^{10,11}. The interplay between tumor aneuploidy/somatic copy number alterations (SCNAs) and the immune response has been demonstrated in advanced BC and other tumor types and can impact both

prognosis and therapy response^{12–15}. However, little is known about the interplay between SCNAs and the patterns of immune cell infiltration in early BC.

Recent methodological advances can greatly facilitate the study of SCNAs and the immune microenvironment by using low-input clinical tumor samples. We recently developed a method, CUTseq, which enables highly multiplexed SCNA profiling at high resolution (10 kilobases, kb) even when using picogram quantities of genomic DNA (gDNA) extracted from small (4–5 mm²) areas in single sections of formalin-fixed paraffin-embedded (FFPE) samples¹⁶. In parallel to sequencing technologies for profiling aneuploidy/SCNAs, emerging automated digital imaging analysis (DIA) technologies, such as multiplexed fluorescent immunohistochemistry (mFHC) and automated TIL enumeration now allow robust identification and quantitation of multiple immune markers even in FFPE tumor tissue sections¹⁷.

Here, we sought to demonstrate the applicability of CUTseq, mFHC and DIA to FFPE BC tissue sections from patients enrolled in the Scandinavian Breast Group (SBG) 2004-1 phase II early BC trial and to portray immuno-genomic correlates detected in these samples.

¹Department of Oncology-Pathology, Karolinska Institutet, Stockholm, Sweden. ²Breast Center, Theme Cancer, Karolinska University Hospital, Stockholm, Sweden. ³Division of Genome Biology, Department of Medical Biochemistry and Biophysics, Karolinska Institutet, Stockholm, Sweden. ⁴Science for Life Laboratory, Stockholm, Sweden. ⁵Department of Pathology and Cytology, Karolinska University Hospital, Stockholm, Sweden. ⁶Department of Pathology, Yale School of Medicine, New Haven, CT, USA. ⁷Department of Immunology, Genetics, and Pathology, Uppsala University, Uppsala, Sweden. ⁸These authors contributed equally: Ioannis Zerdas, Michele Simonetti, Alexios Matikas. ⁹These authors jointly supervised this work: Jonas Bergh, Nicola Crosetto, Theodoros Foukakis. ✉email: jonas.bergh@ki.se; nicola.crosetto@ki.se; theodoros.foukakis@ki.se

RESULTS

Expression patterns of immune cell subsets and related markers

We performed mflHC in 86 out of 124 FFPE samples (69.3%) available from patients initially enrolled in the SBG-2004-1 trial, which were previously arrayed on tissue microarrays (TMA) (Fig. 1a, b and Methods). We assessed the number and spatial location of single-positive (+) CD4 and CD8 T-cells, CD68 + macrophages and FoxP3+ regulatory T-cells as well as their combined expression with the immune checkpoint markers PD-L1 and PD-1 (Fig. 1c). Both in tumor and stromal tissue compartments of matched samples, CD4 + T-cells were the most abundant cell type (mean cell density: 1104 and 909 cells/mm², respectively), followed by CD68 + macrophages (mean cell density: 114.2 and 278.3 cells/mm², respectively) (Fig. 1d and Supplementary Table 1), with higher mean cell densities observed in ER-negative compared to ER-positive tumors (Supplementary Fig. 1a). PD-L1 and PD-1 were mostly expressed in CD4 + T-cells in both intra-tumoral (38.5 cells/mm² and 976.4 cells/mm², respectively) and stromal (55.25 cells/mm² and 779.6 cells/mm², respectively) areas. Stromal PD-1 + CD8 + and PD-1 + CD68 + (254.8 and 217.5 cells/mm², respectively) cell subsets were also expressed at high frequency (Fig. 1e and Supplementary Table 1). Immune cell populations expressing checkpoint proteins were more abundant in ER-negative tumors (Supplementary Fig. 1b). The densities of the different intra-tumoral or stromal immune subtypes were moderately to strongly correlated (Supplementary Table 2). Nevertheless, hierarchical clustering revealed no difference between stromal or tumor-related immune cell clusters (Supplementary Fig. 2). In short, immune checkpoints molecules were expressed both in lymphocytes and macrophages, with a strong propensity for the stromal compartment.

Manual and digital automated evaluation of tumor-infiltrating lymphocytes

We then performed TIL enumeration in whole-tissue sections (WTS) stained with hematoxylin-eosin (H&E) in a total of 93 evaluable samples by eye according to International TILs/Immuno-Oncology Biomarker Working Group Guidelines. The median expression of stromal TILs was 10% (range: 1–90), and high stromal TIL levels were associated with estrogen receptor negativity ($p < 0.001$, Pearson's chi-squared test) and high tumor grade ($p < 0.001$, Pearson's chi-squared test) (Supplementary Table 3). We also tested the performance of an automated TIL scoring algorithm (easTILs, see Methods) in the same tissue slides both in WTS ($n = 88$) and in TMAs ($n = 66$) (Fig. 2). The median score of the easTILs digital evaluation was 12.27% (range: 1.30–62.44% of stroma area) in WTS and 12.95% (range: 1.32–65.29% of stroma area) in TMA. Manual TIL scoring was strongly and statistically significantly correlated with easTILs in WTS (Spearman's $\rho = 0.677$, $p < 0.001$, two-tailed) but not in TMA (Spearman's $\rho = 0.210$, $p = 0.13$, two-tailed) (Fig. 3a–c and Supplementary Table 2). Furthermore, automated TIL evaluation scores were not statistically significantly correlated between WTS and TMAs in patients with matched tissue (Spearman's $\rho = 0.263$, $p = 0.06$, two-tailed) (Fig. 3a and Supplementary Table 2). In the same samples assessed by mflHC, we also examined the correlation between CD4 + and CD8 + stromal cell densities with the extent of TIL infiltration. The mean stromal and intra-tumoral CD4 + and CD8 + T-cell density and their sum (CD4 + and CD8 +) were significantly higher in lymphocytic predominant BC samples (LPBC; stromal TIL > 50%) compared to non-LPBC tumors (Fig. 3d, e and Supplementary Table 2). Similarly, the percentages of automatically counted TILs in WTS and in TMAs were moderately correlated with CD4 + and CD8 + cell densities (Fig. 3a and Supplementary Table 2). These results show that prediction of TIL enumeration by digital

counting depends on tissue source and that mflHC-derived CD4 and CD8 densities are representative of TIL abundance.

SCNA profiling by CUTseq

Out of 96 FFPE samples evaluated by mflHC and/or TILs scoring, 93 samples had gDNA of sufficient quality to be used for CUTseq. As reference for calling SCNAs, we used gDNA extracted from peripheral mononucleated blood cells available for 33 patients (Methods). To assess the reproducibility of CUTseq, we sequenced two libraries prepared using two aliquots of each of the 93 gDNA samples. Forty-four samples reached a sufficient sequencing read depth in both replicates and showed a high correlation of the per bin log₂ ratio up to 100 kilobase resolution (Supplementary Fig. 3a). After copy number calling, we observed a significant correlation (Pearson's $\rho = 0.94$; $p = 2.2 \times 10^{-16}$, two-tailed) of the percentage of the human genome that was amplified or deleted in corresponding replicates and a high concordance of the SNCA profiles between them (Supplementary Fig. 3b, c).

To increase the number of samples, we merged corresponding replicates, which led to 77 out of 93 samples (82.7%) with enough sequencing reads to allow reliable SCNAs calling at 100 kb resolution (see Methods). In these samples, deletions (DEL) were present in higher percentage as compared to amplifications (AMP) (14.6% and 12.2%, respectively) (Fig. 4a). When further subdividing the samples into ER-negative and ER-positive samples we saw similar AMP and DEL percentages (12.4% and 14.9% in ER-positive samples and 11.8% and 14.1% in ER-negative samples, respectively) (Supplementary Fig. 4a). The majority of the alterations were large-sized (>10 megabases, Mb), both in the case of AMP and DEL, followed by medium-sized (1–10 Mb) and focal (<1 Mb) events (Fig. 4b). This was also the case when further stratifying samples by ER status (Supplementary Fig. 4b). AMP occurred most frequently on chromosome 1q, 8q, 17q, 20q, while DEL were predominant on 8p, 11q and 17p (Fig. 4c). We then checked which genes listed in the Catalog of Somatic Mutations in Cancer (COSMIC)¹⁸ were most frequently amplified or deleted. Among these, *MYC* was the most frequently altered gene locus (65% of all the samples) followed by *ERBB2* (57%), *TP53* (48%), *BRCA2* (36%) and *BRCA1* (36%) (Fig. 4c). We also used the GISTIC (Genomic Identification of Significant Targets in Cancer)¹⁹ algorithm to detect significantly focally altered genes. *ERBB2* was the most significantly focally altered gene, followed by *CCND1*, *FGFR1* and *ZNF217* (Fig. 4d, e). Altogether, these results show that high-throughput CUTseq allows robust detection of SCNAs in low-input clinical samples.

Immune-genomic analyses reveal an inverse link between SCNA burden and immune response

We then aimed at deciphering the relationship between the tumoral genomic architecture and the composition of the immune infiltrate. Using unsupervised hierarchical clustering analysis, we detected two distinct genomic groups: cluster 1 ($n = 20$) was characterized by higher SCNA burden (i.e., the percentage of the genome either amplified or deleted) as compared to cluster 2 ($n = 57$), which had a lower SCNA burden (Fig. 5a, b). We did not find any significant difference between the two clusters in terms of overall survival (two-sided log-rank $p = 0.372$). However, we did observe a differential composition of the immune cell infiltrate between the two clusters. The mean distribution of visually scored stromal TILs was significantly lower in cluster 1 as compared to cluster 2 (mean TILs percentage: 9.6% vs. 24.5% in cluster 1 and 2, respectively, $p = 0.016$, Mann-Whitney U test, two-tailed) (Fig. 5d, upper panel). Similarly, the mean percentage expression of all digital TILs variables, in both WTS and TMAs, were higher in cluster 2 (Fig. 5d, upper panel). When we evaluated specific immune cell subsets, we found that intra-tumoral CD4 + and CD68 + cells as well as stromal CD4 +, CD8 + and CD68 + cell abundances were

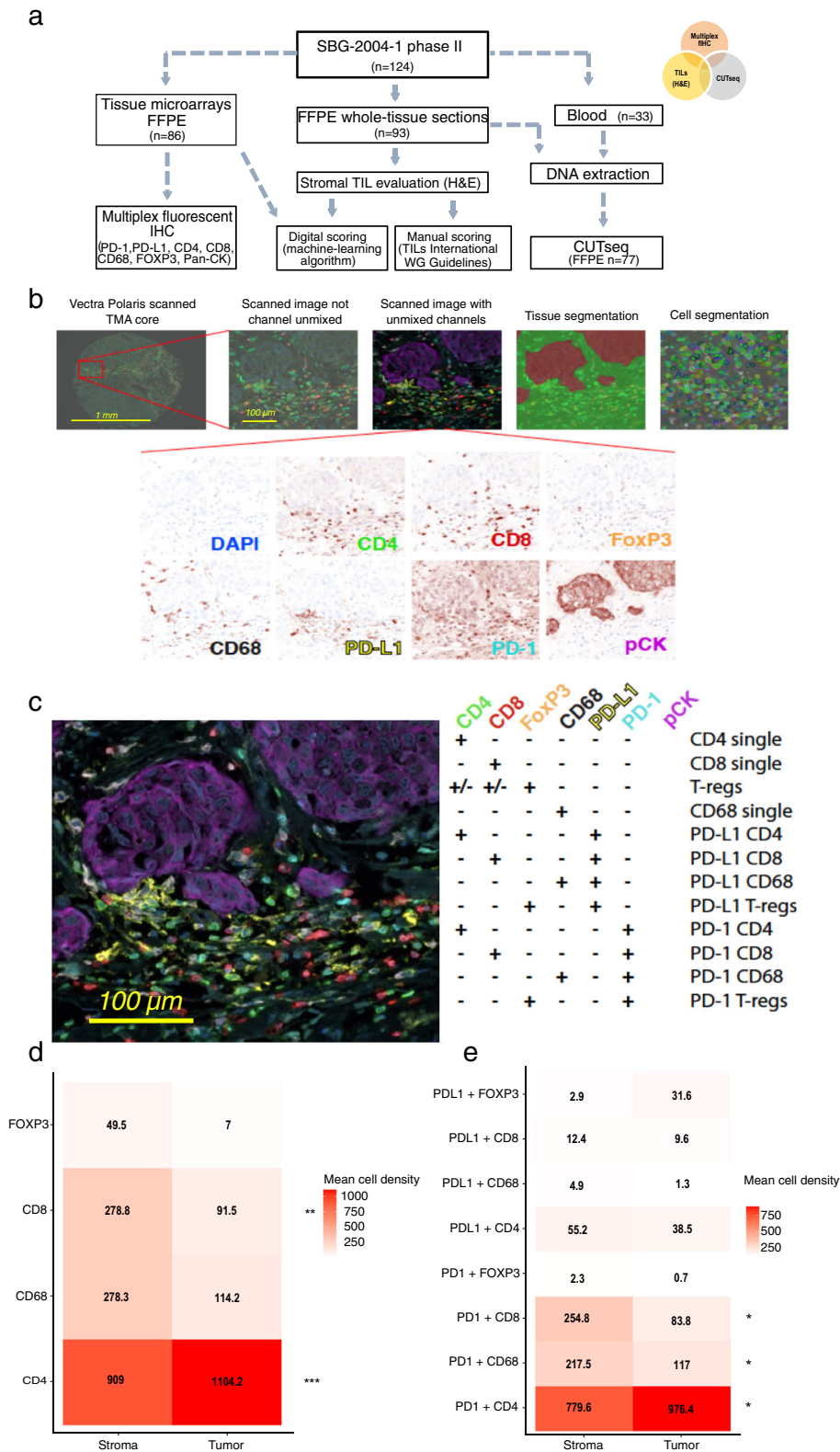


Fig. 1 Immune profiling using a multiplexed method in early breast cancer formalin-fixed paraffin-embedded (FFPE) tissue. **a** Flowchart of the patient sample availability and methods used in the translational sub-study of the SBG-2004-1 early breast cancer trial; **b** Overview and workflow of the multiplexed fluorescent IHC approach in tissue microarrays; **c** Representative image of the spatial immune cell distribution and phenotyping according to the (co)expression of the relevant markers; **d**, **e** Heatmaps depicting mean cell densities of immune cell subpopulations and expression patterns per tissue compartment ($n = 79$).

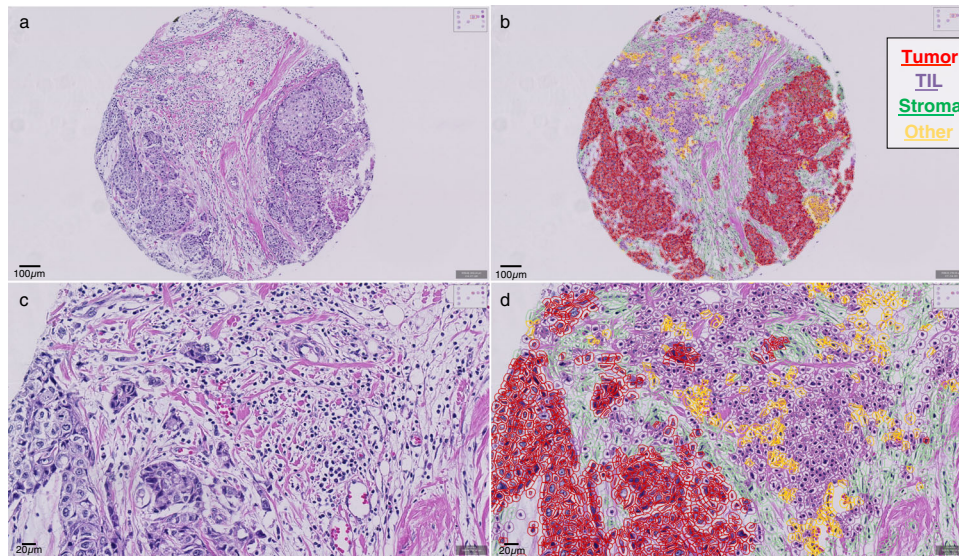


Fig. 2 TILs manual and digital evaluation. Representative image of a tissue-microarray (TMA) core (**a** and **c**, original magnification x200 and x400, respectively); Digital image analysis and different cell type annotations in the same images, using a machine-learning algorithm (**b** and **d**, original magnification x200 and x400, respectively).

significantly increased in cluster 2 (Fig. 5d, middle and lower panels). Altogether, our results indicate that, in early breast cancer tumors, an inflamed tumor microenvironment tends to be associated with a lower SCNA burden and vice versa.

DISCUSSION

This is a correlative and proof-of-principle study that demonstrates the applicability of newly developed methods (CUTseq for SCNA genomic profiling and mflHC and digital image analysis for immune profiling) in archival FFPE tissue, using samples from patients enrolled in the phase II SBG-2004-1 early BC trial. mflHC facilitated the qualitative and quantitative assessment of several markers in a tissue-compartment manner (tumor *versus* stroma area), while digital TILs scoring²⁰ enabled the evaluation of morphology-based immune infiltration on routine H&E-stained sections. Moreover, considering that FFPE tissue remains one of the main sources of patient material for translational cancer research and the inherent challenges related to the isolation of nucleic acids from FFPE samples^{21,22}, we confirmed the ability of CUTseq to yield high-quality SCNA profiles even in old FFPE samples (storage age range: 14–16 years), further highlighting their potential applications. In this cohort of samples, the method successfully detected the loss of 8p, a frequent deletion of breast cancer associated with poor patient survival and cell invasiveness²³. *MYC*, whose deregulation contributes to BC development and progression and is associated with poor outcomes²⁴, represented the most commonly altered gene locus. Not surprisingly, *ERBB2* was also among the most frequently altered loci²⁵.

Advances in quantitative IHC and emerging approaches for multiplexed IHC have shifted the landscape of immune profiling from single to multiple marker evaluation^{17,26} in tumor samples. According to a large meta-analysis, multiplexed IHC/IF better predicts benefit to anti-PD-L1/PD-1 treatment over other biomarker modalities (i.e., TMB or gene-expression profiling)²⁷, supporting the potential clinical utility of multi-marker assessment. Similarly, machine-learning algorithms and digital image analysis approaches provide the potential for intelligent digital pathology applications, accurate diagnostics and biomarker development^{28,29}. The observed correlations between automated assessment of TILs with both manual TIL-WGS scoring³⁰ and mflHC

counts, as well as its feasibility in TMAs could pave the way for its widespread use in translational BC studies. Upon validation in larger cohorts, digital image analysis of TILs could greatly facilitate studies on TILs due to the robust reproducibility and low demand in time and manual labor of this technique^{31–33}. These high-dimensional methods could also provide the tools for further dissection and deconvolution of tumor microenvironment heterogeneity³⁴ and the complex regulation of tumor-host interplay^{35,36}. Whether these specific immune-related patterns correlate to clinical outcomes and confer predictive implications for immunotherapy remain to be explored. Similarly, future applications of CUTseq to larger FFPE sample cohorts could enable the identification of clinically relevant SCNA signatures.

The second focus of our study was to explore the association between tumor SCNAs and the host immune response. Following the first tissue/site-agnostic approval of pembrolizumab for patients with microsatellite instability-high or mismatch repair deficient unresectable or metastatic solid tumors³⁷, the identification of genetic determinants of anti-tumor immune response^{38,39} is potentially clinically meaningful. TMB could trigger immune response and predict longer survival in BC, despite the generally lower mutational load/immunogenicity and increased heterogeneity of this cancer type^{6,40–44}, but its clinical utility still remains questionable. One hypothesis for such association maintains that a greater level of heterogeneity at the genomic and cellular level would lead to a greater number of neoantigens, a stronger immune response and better outcomes. In contrast, it has also been proposed that a low number of infiltrating immune cells causes diminished immune surveillance and immunoeediting and thus leads to increased clonal heterogeneity. Of note, aneuploidy and SCNAs involving either larger or smaller (focal) portions of the genome could also drive diverse cancer hallmarks including cell proliferation and immune escape^{11,13} and thus be associated with dismal prognosis^{45,46}. Furthermore, SCNAs (especially deletions) in antigen presentation related genes could negatively impact lymphocytic infiltration, irrespective of the TMB, which has been shown to increase the number of neoantigens^{13,47}. In this study, we confirmed that a higher SCNA burden is correlated with decreased immune cell infiltration and especially a reduction in stromal TILs. Previous studies have also reported a negative correlation between the SCNA burden

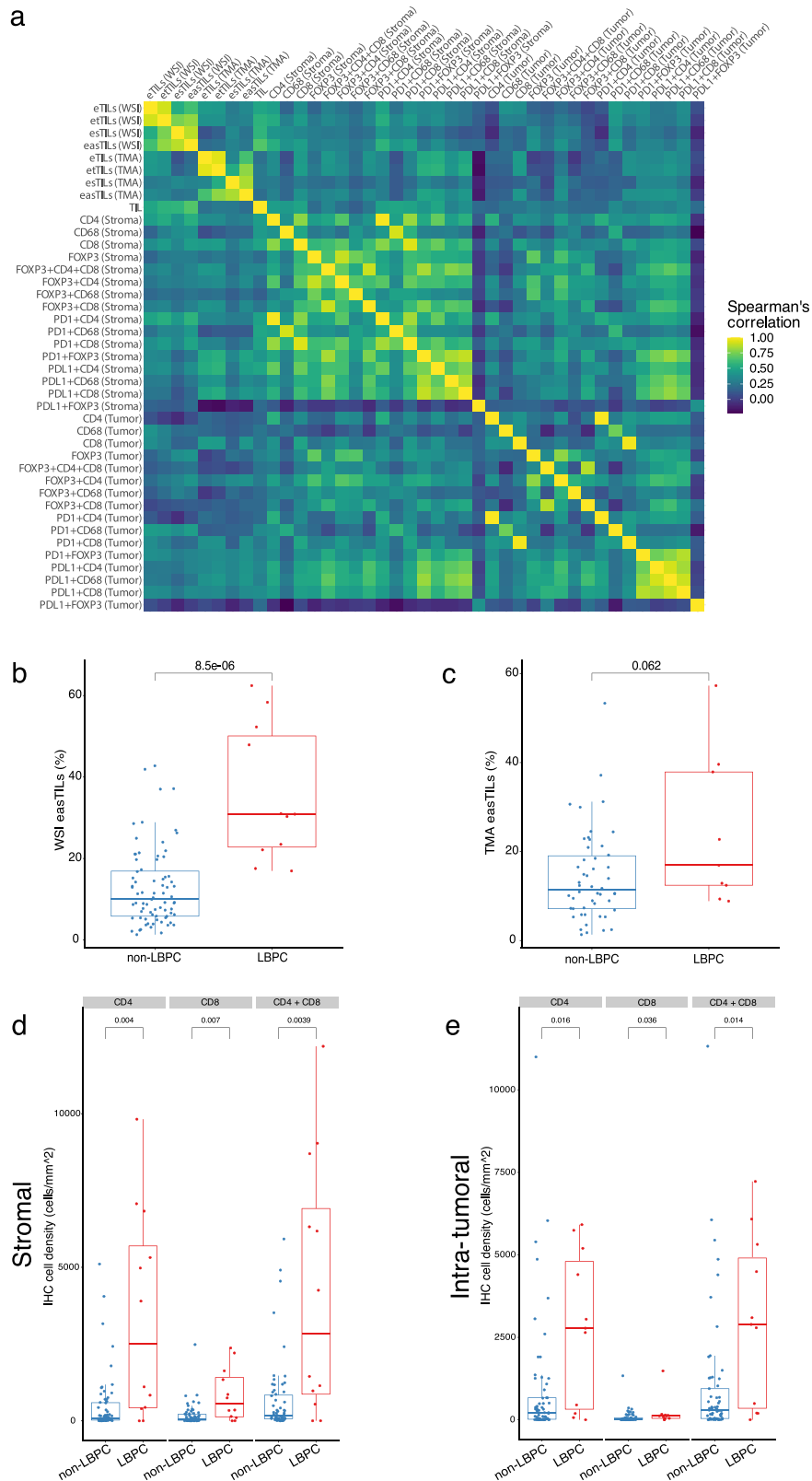


Fig. 3 Correlations of TILs with multiplex IHC. a Correlation matrix of the different variables derived from multiplex fluorescent IHC, manual and digital TILs scoring; Correlations of easTILs in whole-slide images (**b**) and TMA (**c**) with manual TILs scoring in lymphocyte-predominant breast cancer (LPBC) and non-LPBC; Correlation between CD4 and CD8 stromal (**d**) and intra-tumoral (**e**) immune cell subsets with LPBC and non-LPBC based on manual TILs scoring; In the boxplots, each box extends from the 25th to the 75th percentile, the midline represents the median, and the whiskers extend from $-1.5 \times \text{IQR}$ to $+1.5 \times \text{IQR}$ from the closest quartile, where IQR is the inter-quartile range; WSI: whole-slide images, TMA: tissue microarrays.

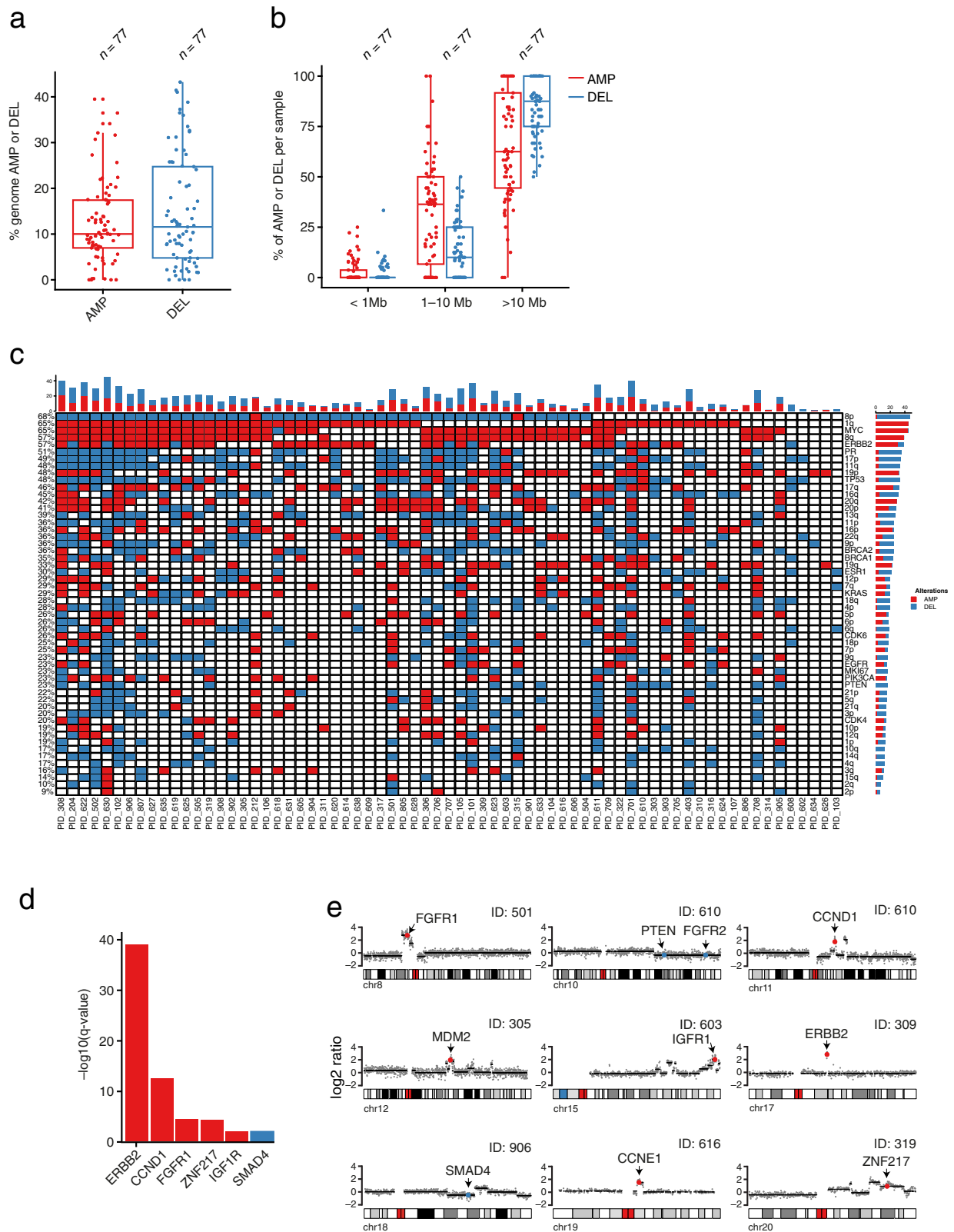


Fig. 4 Copy number alteration distribution and frequency in FFPE samples using the CUTseq method. Percentage (a) and size (b) of the altered genome (amplified or deleted) in the SBG-2004-1 study. In the boxplots, each box extends from the 25th to the 75th percentile, the midline represents the median, and the whiskers extend from $-1.5 \times \text{IQR}$ to $+1.5 \times \text{IQR}$ from the closest quartile, where IQR is the inter-quartile range; **c** Landscape of the most frequently altered chromosomal arm and gene loci among study samples; **d**, **e** Significantly focally altered genes in relation to their chromosomal location.

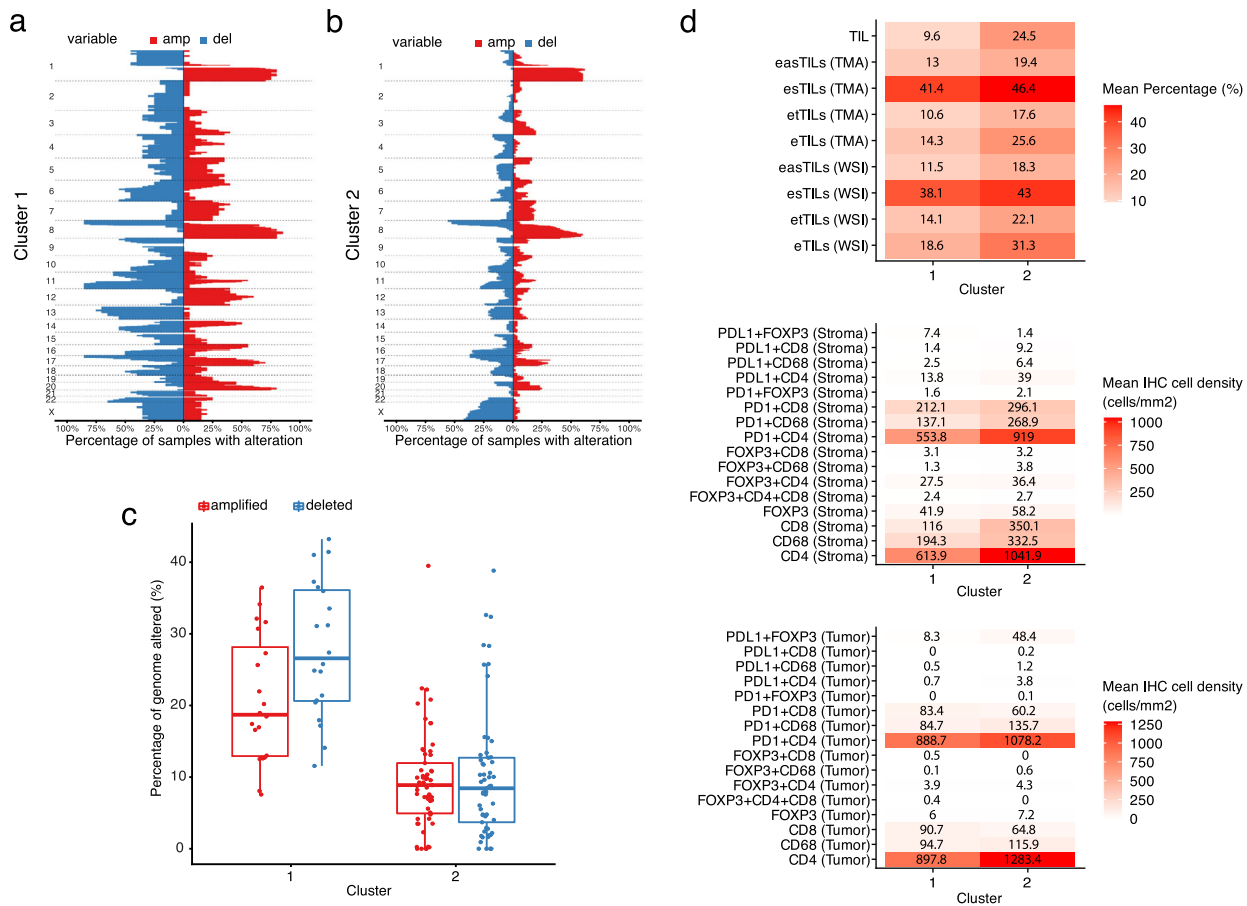


Fig. 5 Combined immunogenomic analysis in the SBG-2004-1 trial. **a, b** CNA clusters and graph depicting the respective CNA burden (percentage of genome amplified/deleted); **c** Distribution of CNA among the distinct genomic clusters. In the boxplots, each box extends from the 25th to the 75th percentile, the midline represents the median, and the whiskers extend from $-1.5 \times$ IQR to $+1.5 \times$ IQR from the closest quartile, where IQR is the inter-quartile range; **d** Heatmaps of the mean cell density and expression of the different multiplex immune cell subsets and H&E TIL variables (both manual and digital TILs) within CNA clusters.

and immune gene signatures in BC, mostly in the triple-negative subtype and for whole chromosome/arm aneuploidy as compared to focal SCNAs, further indicating the role of gene dosage effects^{13–15,48}. In contrast, a weak positive correlation was noted in two other studies, especially in the ER+ subtype^{38,49}. Thus, considering (i) the positive correlation of the TMB with SCNAs¹³, the TMB-independent prognostic significance of SCNAs⁴⁵ as well as (iii) the opposing impact on immune infiltration and response to immunotherapy (SCNAs predicted poorer survival in melanoma patients receiving ICB as compared to TMB¹³) the following question arises: Could a combined immunogenomic score including the SCNA burden, TMB and host immune response better stratify BC patients and predict benefit from immunotherapy?

The present exploratory study suffers from several limitations, which will need to be addressed in follow-up studies. Our small sample size did not enable additional subgroup analyses (e.g., further evaluation of predictive implications regarding dose tailored chemotherapy). The few documented events after a 10-year follow-up precluded the exploration of the prognostic value of our findings. Furthermore, the use of TMAs as compared to whole-tissue sections might underestimate the extent of lymphocytic infiltration and the expression of PD-L1/PD-1 axis^{50,51}, as indirectly supported by the results of TILs enumeration in our study. Finally, since our study was mostly correlative, causality in our observations remains to be proven.

The present proof-of-principle study indicates the feasibility of SCNA and immune cell profiling applications on a large scale using

archival, low-input FFPE BC samples. This could pave the way for further applications and validation in larger patient cohorts, such as the continuation phase III PANTHER trial^{52–55}. Our findings also provide insights into the interplay between SCNAs and the immune microenvironment in patients with early BC. Ultimately, we need to identify whether specific immunogenomic patterns confer poor prognosis despite the use of adjuvant therapy, hence marking a candidate population for treatment escalation using immunomodulating therapies.

METHODS

Study samples

The Scandinavian Breast Group (SBG) 2004-1 study is a randomized phase II study, which aimed to evaluate the feasibility and tolerability of three different adjuvant chemotherapy regimens: (a) tailored according to the hematologic nadirs and dose dense epirubicin, cyclophosphamide and docetaxel (EC → T) every 2 weeks, (b) fixed dose regimen of the same agents every 2 weeks and (c) the TAC regimen (docetaxel, doxorubicin and cyclophosphamide every 3 weeks), enrolling a total of 124 patients with node-positive disease. The patient characteristics and primary safety and efficacy analysis, as well as the long-term follow-up (median: 10.3 years) analysis have been previously reported^{56,57}. The analyses performed in the present study have been approved by the ethics committee at Karolinska Institutet, Stockholm, Sweden (Dnr 2017/345-32 and Dnr 2018/1084-32) and by the Swedish Medical Product Agency (Dnr 5.1 2017–51466). Written informed consent was obtained from all patients prior to enrollment in the clinical trial. The conduct of the study conformed to the standards set by the Declaration of Helsinki. This trial was initiated in 2004, when trial

registration was not compulsory. It is the feasibility study of a randomized phase III trial (PANTHER, EudraCT number 2007-002061-12 and ClinicalTrials.gov accession number NCT00798070).

Patient tissue sample processing and tissue microarray construction

FFPE patient tissue was used for this study (storage age range: 14–16 years); an initial whole-tissue section (WTS) (thickness: 4 μm) was taken from each tissue block and subsequently stained with hematoxylin and eosin (H&E) using standard protocols. The tumor area and cellularity (% of tumor cells) were then annotated and confirmed by a certified pathologist (J.H.). Two additional tissue sections (thickness: 10 μm each) from each patient FFPE sample were also obtained only from the tumor area using scalpels directly on the tissue block. These sections were used for DNA extraction as described hereunder. TMA were also constructed from primary tumors of all patients from the FFPE blocks using an automated tissue microarrayer (VTA-100, Veridiam, Oceanside, CA, USA). Each TMA consisted of duplicate cores per tumor/patient (diameter: 1 mm), originating from the previously annotated tumor-rich areas.

Evaluation of tumor-infiltrating lymphocytes

TILs enumeration. Stromal tumor-infiltrating lymphocytes (TIL) were evaluated on H&E-stained full-face sections, by a certified pathologist (J.H.), who was blinded to other clinicopathological and genomic characteristics, as the percentage (%) of tumor stroma covered by infiltrating lymphocytes, according to the recommendations of the International TILs/Immuno-Oncology Biomarker Working Group³⁰.

Digital-assisted evaluation of TILs. An image-based, automated evaluation of TILs was performed in both H&E-stained whole-slide images (WSI) and TMA, using the QuPath open source software^{20,58,59}. Briefly, a classifier algorithm compatible with the QuPath software has been created in order to define tumor cells, lymphocytes, stromal cells and other cells on the stained sections. For both WSI and TMA the following variable $\text{easTILs}\% = \text{TILs Cell Area} / \text{Stroma Area} * 100$, was calculated as a surrogate of the respective definition from the TILs Working Group for the visual assessment while different calculated variables/scores for the machine-defined TILs are summarized in the Supplementary Table 4.

Multiplex fluorescent immunohistochemical staining

Tissue sections (thickness: 4 μm) were prepared from the FFPE blocks of TMA for the staining with multiplex fluorescent immunohistochemistry (mIHC), enabling the simultaneous and spatial in situ detection of multiple protein markers^{60–62}. Specifically, the custom-based 7-color IHC kit (Opal™ 7 Solid Tumor Immunology Kit, Akoya Biosciences, Marlborough, MA, USA), has been optimized in order to include a panel of 6 immune markers: CD4 (1:100, Cat No. M731029-2), CD8a (1:200, Cat No. MA513473), PD-L1 (1:400, Cat No. ab228462), PD-1 (1:100, Cat No. ab52587), FoxP3 (1:300, Cat No. 12653), CD68 (1:400, Cat No. M087629-2). For improved visualization of epithelial tissue, a cocktail of primary antibodies against E-cadherin (1:2000, Cat No. 610182), cytokeratin (1:400, Cat No. GA05361-2) and pan-cytokeratin (1:500, Cat No. ab7753) was used. The detailed protocol and reagent references of the mIHC procedure in this study are presented in Supplementary Table 5. The fully automated Leica Bond RX™ (Leica Biosystems, Buffalo Grove, IL, USA) was used for the multiplex staining. Tissue sections were stained with 4',6-diamidino-2-phenylindole (DAPI) in order to visualize the nuclei and subsequently mounted with Prolong Diamond Antifade Mountant (ThermoFisher, Waltham, MA, USA).

Image acquisition, analysis, and thresholding of the multispectral approach

Imaging of the TMA was performed using the Vectra® Polaris™ Automated Quantitative Pathology Imaging System (Akoya Biosciences, Marlborough, MA, USA)^{60,61}. A whole-slide scanning (10x) was obtained in order to locate and label the TMA cores using the Phenochart software (Akoya Biosciences, Marlborough, MA, USA). Multispectral fluorescent imaging was then applied on the selected regions providing a resolution of 2 pixels per 1 μm . Spectral unmixing was performed using the inForm® image analysis software (Akoya Biosciences, Marlborough, MA, USA) and the signal intensity for each fluorophore was normalized for exposure. A machine-learning tissue segmentation algorithm was then set up and applied for the image analysis following a training step. This included the manual

annotation of three distinct compartment/region types (tumor, stroma and blank areas) in a training set of TMA cores. Cell segmentation was carried out based on the nuclear DAPI staining and with the surrounding area (3 mm perinuclear) to be defined as the cytoplasm zone. The established image analysis protocol was applied for the complete set of scanned TMA cores ($n = 157$). Each image was manually evaluated by three investigators (I.Z., A.M., P.M.) so as to exclude necrotic areas, non-tumor tissue and/or staining artifacts from subsequent analyses and discrepancies were resolved by a certified pathologist (A.M.). Both nuclear and cytoplasmic areas (making a total cell area) were assessed for markers' expression, except FoxP3, which was evaluated only in nuclear areas. The intensity positivity threshold was defined individually for each biomarker using the built-in function for cell phenotyping (inForm® software) in a randomly selected set of TMA cores (20 images, 100 cells visually determined per marker). These thresholds were applied to the output data from the complete cohort to classify cells according to the expression of each marker either as positive or negative. Duplicate TMA cores belonging to the same tumor were merged and cell infiltration was normalized against the total viable tissue area. The cell density (cells/ mm^2) of each single marker, i.e., number of immune marker-positive cells normalized separately to the tumor and stromal areas/compartments was then computed for each sample. Co-expression patterns of the various immune-positive markers were used for the identification of immune cell subpopulations. The analytical workflow of the applied multispectral method is summarized in Fig. 1b.

DNA extraction from FFPE tumor tissue and blood samples

DNA was extracted from archival FFPE breast cancer patient tissue based on the aforementioned tumor area annotations and description, using the AllPrep DNA/RNA FFPE Kit (Cat. No. 80234, QIAGEN, Germany). Briefly, the main steps of the extraction process involved deparaffinization using xylene, washing in 100% ethanol, air-drying, lysis/digestion using proteinase K, on-column RNAase treatment, genomic DNA binding on QIAmp MinElute spin column, washing and elution of DNA in EB buffer (Cat. No. 19086, QIAGEN, Germany). Germline DNA was extracted also from patients' peripheral blood samples using the FlexiGene DNA kit (Cat No. 51206, QIAGEN, Germany). Quality control (QC) was performed for the estimated yield of the extracted DNA. Concentration and the A_{260}/A_{280} and A_{260}/A_{230} absorbance ratios (purity estimation) were obtained using the spectrophotometer NanoDrop ND-1000 (Saveen Werner, Sweden). Further estimation of the DNA concentration was performed using the Qubit® 3.0 Fluorometer (ThermoFisher Scientific, USA) and the Qubit™ dsDNA BR (Broad Range) Assay kit (Cat No Q32850, Invitrogen, USA). Furthermore, the integrity of DNA was estimated based on the DNA Integrity Number (DIN) values, using the Agilent TapeStation 2200 System (Agilent, Santa Clara, CA, USA) according to the manufacturer's instructions.

CUTseq

We designed and prepared 96 CUTseq adapters as previously described¹⁶. 93/96 gDNA FFPE samples and 33/36 gDNA blood samples were used (remaining samples were excluded due to low concentration) and two technical replicates were prepared by two different operators. Upon receipt samples were diluted to a concentration of approximately 18 ng/ μl . The experiment was performed on a 384-well plate divided into four different parts: (1) top left 96 wells were used for 92 gDNA FFPE samples (replicate 1) and 4 negative control (Nuclease Free Water); (2) top right 96 wells were used for 33 gDNA blood samples (replicate 1) and 3 negative control (Nuclease Free Water); (3) bottom left 96 wells were used for 92 gDNA FFPE samples (replicate 2) and 4 negative control (Nuclease Free Water); (4) bottom right 96 wells were used for 33 gDNA blood samples (replicate 2) and 3 negative control (Nuclease Free Water). First 5 μl of Vapor Lock (Qiagen, Cat.No. 981611) was dispensed in each well to prevent evaporation. After this we used the I-DOT One robot for all subsequent dispensing steps. We dispensed 350 nl of gDNA (concentration around 6.3 ng) from FFPE and blood samples and 350 nl of Nuclease Free Water as control. Digestion mix containing 50 nl of CutSmart buffer (NEB, Cat. no. B7204S) and 100 nl of NlaIII-HF enzyme (NEB, Cat. no. R0125L). Plate was centrifuged at 1200 $\times g$ for 5 min. Digestion was performed at 37 °C for 30 min followed by 20 min at 65 °C to inactivate the enzyme. After digestion, we dispensed 300 nl of 33 nM CUT adapter together with 700 nl of ligation mix containing 200 nl of T4 rapid DNA ligase (Thermo Fisher Scientific, Cat.No. K1423), 300 nl of T4 ligase buffer (Thermo Fisher Scientific, Cat. No. K1423), 120 nl of 10 mM ATP (Thermo Fisher Scientific, Cat.No. PV3227), 30 nl of 50 mg/ml bovine serum albumin (Thermo Fisher Scientific, Cat.No. AM2616),

and 50 nl of nuclease-free water (Thermo Fisher Scientific, Cat.No. 4387936) and the plate was incubated at 25 °C for 30 min. After ligation, we added 5 µl of 1xPBS (Thermo Fisher Scientific, Cat.No. AM9625) to each well and pooled the contents of every well (keeping the four different parts separate) with different barcodes in four different eppendorf tubes. From this step the two replicates were performed by two different operators. After short spin, Vapor-Lock (top layer) was removed and purification was carried out by adding 3.7 µl of 20 mg/ml glycogen (Sigma, Cat.No. 10901393001), 11.5 µl of 3 M sodium acetate (Life Technologies, Cat.No. AM9740) and 288 µl of ice-cold Absolute Ethanol (VWR, Cat.No. 20816.367) per 100 µl of DNA solution and incubate at −80 °C overnight. The next day Ethanol precipitation was performed and DNA sonicated using Covaris ME220 Focused-ultrasonicator with the target peak of 200 bp. Sheared DNA was purified with 1.3X ratio of Agencourt Ampure XP beads (Beckman Coulter, Cat. No. A63881). Eight microliters of purified DNA was used as input for the IVT step and library preparation as described in the original CUTseq paper¹⁶. Final libraries were sequenced on a Illumina NextSeq 500 platform with high output 75 bp single-end kit (Illumina, catalog number FC-404-2005).

Sequencing data processing and copy number calling

We filtered reads based on the presence of the correct prefix, allowing for 1 mismatch in the restriction site. Following this, we removed the barcode and unique molecular identifier (UMI) from the read and appended to the read header using *umi_tools extract* (version 1.1.1)⁶³. Subsequently, we demultiplexed the reads based on the extracted barcodes using *BAMMap demuxbyname* (version 38.76) (<https://sourceforge.net/projects/bbmap>). Demultiplexed reads were then aligned to the human reference genome GRCh37/hg19 using Burrows-Wheeler Aligner (BWA) (version 0.7.17-r1188)⁶⁴. Aligned reads were position sorted and deduplicated with *samtools sort* (version 1.10)⁶⁵ and *umi_tools dedup* (version 1.1.1)⁶³, respectively. The preprocessing pipeline used in this study is made available through a snakemake file on <https://github.com/ljwharbers/sbg2004-cutseq>.

We called somatic copy number variants using a pipeline from the Genome Analysis ToolKit (GATK) (version 4.1.8.0)⁶⁶. In short, we produced a list of annotated intervals using *PreprocessIntervals* and *AnnotateIntervals*. Reads were counted in these intervals using *CollectReadCounts* and a Panel Of Normal of 33 blood samples was created using *CreateReadCountPanelOfNormals*. Tumor profiles were normalized and segments were modeled using *DenoiseReadCounts* and *ModelSegments*, respectively. Finally, significantly amplified or lost segments were called using *CallCopyRatioSegments*. The copy number variant pipeline with the exact parameters used is made available through a snakemake file on <https://github.com/ljwharbers/sbg2004-cutseq>.

Data processing and statistical analyses

For comparison of immune cell densities groups of paired samples between tumor and stroma area, the Wilcoxon signed-rank test was used. Descriptive statistics (mean, standard deviation, median) were used for continuous variables (e.g., mFIHC cell densities, eTILs). Unsupervised hierarchical clustering was performed on normalized data in order to identify CNA (based on the called segments of the bins) and/or immune cell clusters. Associations of different immune cell patterns (including TILs expression levels) and DNA copy number alterations with clinicopathological parameters were performed using chi-square (χ^2), Fisher's exact or Mann-Whitney *U*-tests, where appropriate. The association between TIL enumeration using manual and automated counting was assessed using Spearman correlation. The observed number of survival events in each CNA group was compared using the log-rank test. All analyses were performed using SPSS (v.25.0 Corp. Armonk, NY, USA), R studio (version 4.3) and GraphPad Prism (version 8.0. GraphPad software Inc., San Diego, CA, USA).

Reporting summary

Further information on research design is available in the Nature Research Reporting Summary linked to this article.

DATA AVAILABILITY

The segmented SCNA profiles are available in the Supplementary Material (Supplementary Data 1). The raw data files (BAM) and other data that support the findings of this study are available from the corresponding authors (J.B., N.C., T.F.)

upon reasonable request and provided that the intended use is in accordance with the ethics approval and the informed consent signed by the trial participants.

CODE AVAILABILITY

All the custom code used to process and analyze the sequencing data is also available at the following GitHub link: <https://github.com/ljwharbers/sbg2004-cutseq>.

Received: 18 May 2021; Accepted: 21 October 2021;

Published online: 19 November 2021

REFERENCES

- Schmid, P. et al. Atezolizumab and nab-paclitaxel in advanced triple-negative breast cancer. *N. Engl. J. Med.* **379**, 2108–2121 (2018).
- Miles, D. et al. LBA15 primary results from IMpassion131, a double-blind placebo-controlled randomised phase III trial of first-line paclitaxel (PAC)±atezolizumab (atezo) for unresectable locally advanced/metastatic triple-negative breast cancer (mTNBC). *Ann. Oncol.* **31**, S1147–S1148 (2020).
- Matikas, A. et al. Prognostic Implications of PD-L1 expression in breast cancer: systematic review and meta-analysis of immunohistochemistry and pooled analysis of transcriptomic data. *Clin. Cancer Res.* <https://doi.org/10.1158/1078-0432.CCR-19-1131> (2019).
- Matikas, A. et al. Dynamic evaluation of the immune infiltrate and immune function genes as predictive markers for neoadjuvant chemotherapy in hormone receptor positive, HER2 negative breast cancer. *Oncoimmunology* **7**, e1466017 (2018).
- Denkert, C. et al. Tumour-infiltrating lymphocytes and prognosis in different subtypes of breast cancer: a pooled analysis of 3771 patients treated with neoadjuvant therapy. *Lancet Oncol.* **19**, 40–50 (2018).
- Karn, T. et al. Tumor mutational burden and immune infiltration as independent predictors of response to neoadjuvant immune checkpoint inhibition in early TNBC in GeparNuevo. *Ann. Oncol.* **31**, 1216–1222 (2020).
- Foukakis, T. et al. Immune gene expression and response to chemotherapy in advanced breast cancer. *Br. J. Cancer* **118**, 480–488 (2018).
- Adams, S. et al. Pembrolizumab monotherapy for previously treated metastatic triple-negative breast cancer: cohort A of the phase II KEYNOTE-086 study. *Ann. Oncol.* **30**, 397–404 (2019).
- Franzoi, M. A., Romano, E. & Piccart, M. Immunotherapy for early breast cancer: too soon, too superficial, or just right?. *Ann. Oncol.* **32**, 323–336 (2021).
- Hanahan, D. & Weinberg, R. A. Hallmarks of cancer: the next generation. *Cell* **144**, 646–674 (2011).
- Ben-David, U. & Amon, A. Context is everything: aneuploidy in cancer. *Nat. Rev. Genet.* **21**, 44–62 (2020).
- Braun, D. A. et al. Interplay of somatic alterations and immune infiltration modulates response to PD-1 blockade in advanced clear cell renal cell carcinoma. *Nat. Med.* **26**, 909–918 (2020).
- Davoli, T., Uno, H., Wooten, E. C. & Elledge, S. J. Tumor aneuploidy correlates with markers of immune evasion and with reduced response to immunotherapy. *Science* **355**, <https://doi.org/10.1126/science.aaf8399> (2017).
- Karn, T. et al. Association between genomic metrics and immune infiltration in triple-negative breast cancer. *JAMA Oncol.* **3**, 1707–1711 (2017).
- Xiao, Y. et al. Multi-omics profiling reveals distinct microenvironment characterization and suggests immune escape mechanisms of triple-negative breast cancer. *Clin. Cancer Res.: Off. J. Am. Assoc. Cancer Res.* **25**, 5002–5014 (2019).
- Zhang, X. et al. CUTseq is a versatile method for preparing multiplexed DNA sequencing libraries from low-input samples. *Nat. Commun.* **10**, 4732 (2019).
- Taube, J. M. et al. The Society for Immunotherapy of Cancer statement on best practices for multiplex immunohistochemistry (IHC) and immunofluorescence (IF) staining and validation. *J. Immunother. Cancer* **8**, <https://doi.org/10.1136/jitc-2019-000155> (2020).
- Forbes, S. A. et al. COSMIC: somatic cancer genetics at high-resolution. *Nucleic Acids Res.* **45**, D777–d783 (2017).
- Mermel, C. H. et al. GISTIC2.0 facilitates sensitive and confident localization of the targets of focal somatic copy-number alteration in human cancers. *Genome Biol.* **12**, R41 (2011).
- Acs, B. et al. An open source automated tumor infiltrating lymphocyte algorithm for prognosis in melanoma. *Nat. Commun.* **10**, 5440 (2019).
- Greytak, S. R., Engel, K. B., Bass, B. P. & Moore, H. M. Accuracy of molecular data generated with FFPE biospecimens: lessons from the literature. *Cancer Res.* **75**, 1541–1547 (2015).
- Kresse, S. H. et al. Evaluation of commercial DNA and RNA extraction methods for high-throughput sequencing of FFPE samples. *PLoS ONE* **13**, e0197456 (2018).

23. Cai, Y. et al. Loss of chromosome 8p governs tumor progression and drug response by altering lipid metabolism. *Cancer Cell* **29**, 751–766 (2016).
24. Xu, J., Chen, Y. & Olopade, O. I. MYC and breast cancer. *Genes Cancer* **1**, 629–640 (2010).
25. Harari, D. & Yarden, Y. Molecular mechanisms underlying ErbB2/HER2 action in breast cancer. *Oncogene* **19**, 6102–6114 (2000).
26. Yaghoobi, V. et al. Advances in quantitative immunohistochemistry and their contribution to breast cancer. *Expert Rev. Mol. Diagn.* **20**, 509–522 (2020).
27. Lu, S. et al. Comparison of biomarker modalities for predicting response to PD-1/PD-L1 checkpoint blockade: a systematic review and meta-analysis. *JAMA Oncol.* **5**, 1195–1204 (2019).
28. Acs, B., Rantalainen, M. & Hartman, J. Artificial intelligence as the next step towards precision pathology. *J. Intern. Med.* **288**, 62–81 (2020).
29. Bera, K., Schalper, K. A., Rimm, D. L., Velcheti, V. & Madabhushi, A. Artificial intelligence in digital pathology—new tools for diagnosis and precision oncology. *Nat. Rev. Clin. Oncol.* **16**, 703–715 (2019).
30. Salgado, R. et al. The evaluation of tumor-infiltrating lymphocytes (TILs) in breast cancer: recommendations by an International TILs Working Group 2014. *Ann. Oncol.* **26**, 259–271 (2015).
31. Klauschen, F. et al. Scoring of tumor-infiltrating lymphocytes: From visual estimation to machine learning. *Semin. Cancer Biol.* **52**, 151–157 (2018).
32. Amgad, M. et al. Report on computational assessment of Tumor Infiltrating Lymphocytes from the International Immunology Biomarker Working Group. *NPJ Breast Cancer* **6**, 16 (2020).
33. Kos, Z. et al. Pitfalls in assessing stromal tumor infiltrating lymphocytes (sTILs) in breast cancer. *NPJ Breast Cancer* **6**, 17 (2020).
34. Chuah, S. & Chew, V. High-dimensional immune-profiling in cancer: implications for immunotherapy. *J. Immunother. Cancer* **8**, <https://doi.org/10.1136/jitc-2019-000363> (2020).
35. Zerdes, I., Matikas, A., Bergh, J., Rassidakis, G. Z. & Foukakis, T. Genetic, transcriptional and post-translational regulation of the programmed death protein ligand 1 in cancer: biology and clinical correlations. *Oncogene* **37**, 4639–4661 (2018).
36. Chretien, S., Zerdes, I., Bergh, J., Matikas, A. & Foukakis, T. Beyond PD-1/PD-L1 inhibition: what the future holds for breast cancer immunotherapy. *Cancers* **11**, <https://doi.org/10.3390/cancers11050628> (2019).
37. U.S. Food and Drug Administration. *FDA Grants Accelerated Approval to Pembrolizumab for First Tissue/site Agnostic Indication*. (US Food and Drug Administration, 2017).
38. Budczies, J. et al. Integrated analysis of the immunological and genetic status in and across cancer types: impact of mutational signatures beyond tumor mutational burden. *Oncoimmunology* **7**, e1526613 (2018).
39. Keenan, T. E., Burke, K. P. & Van Allen, E. M. Genomic correlates of response to immune checkpoint blockade. *Nat. Med.* **25**, 389–402 (2019).
40. Thomas, A. et al. Tumor mutational burden is a determinant of immune-mediated survival in breast cancer. *Oncoimmunology* **7**, e1490854 (2018).
41. Yarchoan, M., Hopkins, A. & Jaffee, E. M. Tumor mutational burden and response rate to PD-1 inhibition. *N. Engl. J. Med.* **377**, 2500–2501 (2017).
42. Barroso-Sousa, R. et al. Tumor mutational burden and PTEN alterations as molecular correlates of response to PD-1/L1 blockade in metastatic triple-negative breast cancer. *Clin. Cancer Res.: Off. J. Am. Assoc. Cancer Res.* **26**, 2565–2572 (2020).
43. Alexandrov, L. B. et al. Signatures of mutational processes in human cancer. *Nature* **500**, 415–421 (2013).
44. Chan, T. A. et al. Development of tumor mutation burden as an immunotherapy biomarker: utility for the oncology clinic. *Ann. Oncol.* **30**, 44–56 (2019).
45. Hieronymus, H. et al. Tumor copy number alteration burden is a pan-cancer prognostic factor associated with recurrence and death. *Elife* **7**, <https://doi.org/10.7554/eLife.37294> (2018).
46. Smith, J. C. & Sheltzer, J. M. Systematic identification of mutations and copy number alterations associated with cancer patient prognosis. *Elife* **7**, <https://doi.org/10.7554/eLife.39217> (2018).
47. Bassaganyas, L. et al. Copy-number alteration burden differentially impacts immune profiles and molecular features of hepatocellular carcinoma. *Clin. Cancer Res.: Off. J. Am. Assoc. Cancer Res.* **26**, 6350–6361 (2020).
48. Bense, R. Inverse relationships between high somatic copy number load and immune phenotypes in breast cancer. *Cancer Res.* **76**(4 Suppl), Abstract nr P6-08-01 (2016).
49. Safonov, A. et al. Immune gene expression is associated with genomic aberrations in breast cancer. *Cancer Res.* **77**, 3317–3324 (2017).
50. Sobral-Leite, M. et al. Assessment of PD-L1 expression across breast cancer molecular subtypes, in relation to mutation rate, BRCA1-like status, tumor-infiltrating immune cells and survival. *Oncoimmunology* **7**, e1509820 (2018).
51. Castaneda, C. A. et al. Tumor infiltrating lymphocytes in triple negative breast cancer receiving neoadjuvant chemotherapy. *World J. Clin. Oncol.* **7**, 387–394 (2016).
52. Foukakis, T. et al. Effect of tailored dose-dense chemotherapy vs standard 3-weekly adjuvant chemotherapy on recurrence-free survival among women with high-risk early breast cancer: a randomized clinical trial. *Jama* **316**, 1888–1896 (2016).
53. Papakonstantinou, A. et al. Efficacy and safety of tailored and dose-dense adjuvant chemotherapy and trastuzumab for resected HER2-positive breast. *Cancer* **126**, 1175–1182 (2020).
54. Papakonstantinou, A. et al. Neutropenic complications in the PANTHER phase III study of adjuvant tailored dose-dense chemotherapy in early breast cancer. *Acta Oncol.* **59**, 75–81 (2020).
55. Matikas, A. et al. Dose tailoring of adjuvant chemotherapy for breast cancer based on hematologic toxicities: further results from the prospective PANTHER study with focus on obese patients. *Ann. Oncol.* **30**, 109–114 (2019).
56. Margolin, S. et al. A randomised feasibility/phase II study (SBG 2004-1) with dose-dense/tailored epirubicin, cyclophosphamide (EC) followed by docetaxel (T) or fixed dosed dose-dense EC/T versus T, doxorubicin and C (TAC) in node-positive breast cancer. *Acta Oncol.* **50**, 35–41 (2011).
57. Matikas, A. et al. Long-term safety and survival outcomes from the Scandinavian Breast Group 2004-1 randomized phase II trial of tailored dose-dense adjuvant chemotherapy for early breast cancer. *Breast Cancer Res. Treat.* **168**, 349–355 (2018).
58. Bai, Y. et al. Abstract P3-08-12: An open source, automated tumor infiltrating lymphocyte algorithm for prognosis in triple-negative breast cancer. *Cancer Res.* **80**, P3-08-12, <https://doi.org/10.1158/1538-7445.SABCS19-P3-08-12> (2020).
59. Bankhead, P. et al. QuPath: Open source software for digital pathology image analysis. *Sci. Rep.* **7**, 16878 (2017).
60. Mezheyeuski, A. et al. Multispectral imaging for quantitative and compartment-specific immune infiltrates reveals distinct immune profiles that classify lung cancer patients. *J. Pathol.* **244**, 421–431 (2018).
61. Lundgren, S. et al. Quantitative, qualitative and spatial analysis of lymphocyte infiltration in periampullary and pancreatic adenocarcinoma. *Int. J. Cancer* **146**, 3461–3473 (2020).
62. Lundgren, S. et al. Topographical distribution and spatial interactions of innate and semi-innate immune cells in pancreatic and other periampullary adenocarcinoma. *Front. Immunol.* **11**, 558169 (2020).
63. Smith, T., Heger, A. & Sudbery, I. UML-tools: modeling sequencing errors in Unique Molecular Identifiers to improve quantification accuracy. *Genome Res.* **27**, 491–499 (2017).
64. Li, H. Aligning sequence reads, clone sequences and assembly contigs with BWA-MEM. Preprint at <https://arxiv.org/abs/1303.3997>(2013).
65. Li, H. et al. The sequence alignment/map format and SAMtools. *Bioinformatics* **25**, 2078–2079 (2009).
66. McKenna, A. et al. The genome analysis toolkit: a mapreduce framework for analyzing next-generation DNA sequencing data. *Genome Res.* **20**, 1297–1303 (2010).

ACKNOWLEDGEMENTS

This work was supported by grants from the Swedish Cancer Society (grant no. CAN 2018/728), the Strategic Research Programme in Cancer (StratCan) at Karolinska Institutet (grant no. 2201) and the Swedish Foundation for Strategic Research (grant no. BD15_0095) to N.C.; by grants from the Stockholm Region (clinical postdoctoral appointment, dnr K 2017-4577) and the Percy Falk Foundation to A.M.; by grants by the Swedish Cancer Society (grant number CAN 2018/846 and Senior Clinical Investigator award CAN 2017/1043) and the Cancer Society in Stockholm (174113) to T.F.; by a grant from the Swedish Breast Cancer Association to T.F. and I.Z. Jonas Bergh's research group receives funding from the Stockholm region, the Swedish Cancer Society, the funds at Radiumhemmet, the Swedish Research Council and the Knut and Alice Wallenberg Foundation. The authors would also like to acknowledge the contribution of Georgia Kokaraki, lab engineer for their technical support with patient material (TMAs) and Markella Zacharouli, Dr. Emmanouil G. Sifakis and Dr. Nicholas P. Tobin for their assistance and useful input in the bioinformatics analyses. Part of this study was presented as a poster form at the San Antonio Breast Cancer Symposium (SABCS) 2020.

AUTHOR CONTRIBUTIONS

Conceptualization: I.Z., A.M., J.B., N.C., T.F.; *Clinical samples:* I.Z., M.S., D.S., S.A., J.B.; *Data curation:* I.Z., M.S., L.H., C.B., B.A., A.M., J.H.; *Formal analysis:* L.H., A.M.; *Funding acquisition:* A.M., J.B., N.C., T.F.; *Investigation:* I.Z., M.S., L.H., A.M., D.S., C.B., B.A., A.M.; *Methodology:* I.Z., M.S., L.H., C.B., B.A., Y.B., D.R., A.M., J.H.; *Project administration:* I.Z., S. A.; *Software:* S.G.; *Supervision:* N.C., T.F.; *Validation:* I.Z., M.S., D.S., A.M.; *Visualization:* I.Z., M.S., L.H., A.M., B.A.; *Writing:* I.Z., M.S., A.M., N.C., T.F.; *Manuscript review and approval:* All authors.

FUNDING

Open access funding provided by Karolinska Institute.

COMPETING INTERESTS

I.Z., M.S., A.M., L.H., N.Z., D.S., C.B., B.A., S.A., P.M.-R., Y.B., A.M., and N.C. have no conflicts of interest to disclose. D.L.R. has served as an advisor for Astra Zeneca, Agendia, Amgen, BMS, Cell Signaling Technology, Cepheid, Danaher, Daiichi Sankyo, Genoptix/Novartis, GSK, Konica Minolta, Merck, NanoString, PAIGE.AI, Perkin Elmer, Roche, Sanofi, Ventana and Ultivue. Amgen, Cepheid, NavigateBP, NextCure, and Konica Minolta fund research in D.L.R.'s lab; J.H.: speakers honorarium and travel support from Roche, Novartis, AstraZeneca, MSD. Institutional research support from Cepheid; J.B. receives research funding from Merck paid to Karolinska Institutet and from Amgen, Bayer, Pfizer, Roche and Sanofi-Aventis paid to Karolinska University Hospital. No personal payments. Payment from UpToDate for a chapter in breast cancer prediction paid to Asklepios Medicine HB. T.F.: institutional grants from Roche and Pfizer and personal fees from Affibody, Novartis, Pfizer, Roche, Exact Sciences, Veracyte, and UpToDate.

ADDITIONAL INFORMATION

Supplementary information The online version contains supplementary material available at <https://doi.org/10.1038/s41523-021-00352-3>.

Correspondence and requests for materials should be addressed to Jonas Bergh, Nicola Crosetto or Theodoros Foukakis.

Reprints and permission information is available at <http://www.nature.com/reprints>

Publisher's note Springer Nature remains neutral with regard to jurisdictional claims in published maps and institutional affiliations.



Open Access This article is licensed under a Creative Commons Attribution 4.0 International License, which permits use, sharing, adaptation, distribution and reproduction in any medium or format, as long as you give appropriate credit to the original author(s) and the source, provide a link to the Creative Commons license, and indicate if changes were made. The images or other third party material in this article are included in the article's Creative Commons license, unless indicated otherwise in a credit line to the material. If material is not included in the article's Creative Commons license and your intended use is not permitted by statutory regulation or exceeds the permitted use, you will need to obtain permission directly from the copyright holder. To view a copy of this license, visit <http://creativecommons.org/licenses/by/4.0/>.

© The Author(s) 2021